JOURNAL OF GEOPHYSICAL RESEARCH, VOL. 112, B08404, doi:10.1029/2006JB004683, 2007

Present-day stress field in the Gibraltar Arc (western Mediterranean)

F. Fernández-Ibáñez,[1] J. I. Soto,[1] M. D. Zoback,[2] and J. Morales[3]

Received 7 August 2006; revised 24 March 2007; accepted 23 April 2007; published 1 August 2007.

[1] The Gibraltar Arc in the western Mediterranean consists of the Betic and Rif Alpine chains and the Alboran Sea Basin. Four types of stress indicators (wellbore breakouts, earthquake focal plane mechanisms, young geologic fault slip data, and hydraulic fracture orientations) indicate a regional NW–SE compressive stress field resulting from Africa-Eurasia plate convergence. In some particular regions, deviations of S_{Hmax} are observed with respect to the regional stress field. They are gentle-to-moderate (22°–36°) anticlockwise rotations located along the North Alboran margin and moderate-to-significant (36°–78°) clockwise rotations around the Trans-Alboran Shear Zone (TASZ). This is a broad fault zone composed of different left-lateral strike-slip fault segments running from the eastern Betics to the Alhoceima region in the Rif and resulting in a major bathymetric high in the Alboran Sea (the Alboran Ridge fault zone). Some of these stress rotations appear to be controlled by steep gradients of crustal thickness variation across the North Alboran margin and/or differential loading imposed by thick sedimentary accumulations in basin depocenters parallel to the shoreline. Other stress perturbations may be related to active left-lateral, strike-slip deformation within the TASZ that crosscuts the entire orogenic arc on a NE–SW trend and represents a key element to understand present-day deformation partitioning in the western Mediterranean.

Citation: Fernández-Ibáñez, F., J. I. Soto, M. D. Zoback, and J. Morales (2007), Present-day stress field in the Gibraltar Arc (western Mediterranean), *J. Geophys. Res.*, *112*, B08404, doi:10.1029/2006JB004683.

1. Introduction

[2] In the western Mediterranean, the Gibraltar Arc (Figure 1) is defined by the arcuate, Alpine orogenic belt formed by the Betic and Rif chains, where studies suggest a complex pattern of recent deformation and stress [e.g., *Rebai et al.*, 1992; *Buforn et al.*, 1995, 2004; *Galindo-Zaldívar et al.*, 1993, 2003; *Stich et al.*, 2003, 2006; *Fadil et al.*, 2006]. Orogenic arcs are commonly characterized by a fan-shaped pattern of the maximum horizontal stress, indicating compression radial to the orogen. This type of stress pattern has been found in active orogenic arcs like the Alps [e.g., *Delacou et al.*, 2004; *Kastrup et al.*, 2004; *Jiménez-Munt et al.*, 2005; *Selverstone*, 2005], the Carpathians [e.g., *Bada et al.*, 1998; *Kovác et al.*, 2002], the Himalayan-Tibet region [e.g., *England and Houseman*, 1986; *Houseman and England*, 1993; *England and Molnar*, 2005], the Andes [e.g., *Coblentz and Richardson*, 1996; *Meijer et al.*, 1997; *Khazaradze and Klotz*, 2003], and the Hellenic Arc [e.g., *Jackson and McKenzie*, 1988; *Mercier et al.*, 1989; *Jackson*, 1994; *Cocard et al.*, 1999]. We have compiled a multidisciplinary data set of 64 well-constrained stress indicators in order to characterize the present-day stress field in the Gibraltar Arc and supplement earthquake focal mechanism data [e.g., *Udías and Buforn*, 1991; *Henares et al.*, 2003; *Stich et al.*, 2003; *Buforn et al.*, 2004] or data inferred from mechanical modeling [e.g., *Jiménez-Munt et al.*, 2001; *Negredo et al.*, 2002].

[3] In section 3, we describe the present-day stress field by combining borehole breakout analysis and data on earthquake focal mechanisms, hydraulic fracturing and Quaternary faults. All the data have been treated according to the guidelines and quality ranking criteria of the World Stress Map [*Zoback and Zoback*, 1991]. On the basis of this data set, we discuss the active processes occurring in this Alpine orogenic arc and how the present-day stress pattern is potentially affected by interactions among different types of processes: (1) ongoing convergence between Eurasia and Africa (~4.5–5.0 mm yr^{-1} with 135°–120° azimuth; according to NUVEL-1A [*DeMets et al.*, 1994]); and (2) secondary sources of stress imposed by variations of crustal structure (in places characterized by abrupt crustal thickness variations) and significant sedimentary accumulations (e.g., >8 km in the West Alboran Basin). We also discuss whether active strike-slip faulting (left-lateral) within a narrow zone of deformation crosscutting

[1] Departamento de Geodinámica and Instituto Andaluz de Ciencias de la Tierra, Universidad de Granada, Granada, Spain.
[2] Department of Geophysics, Stanford University, Stanford, California, USA.
[3] Instituto Andaluz de Geofísica, Universidad de Granada, Granada, Spain.

0148-0227/07/2006JB004683$09.00

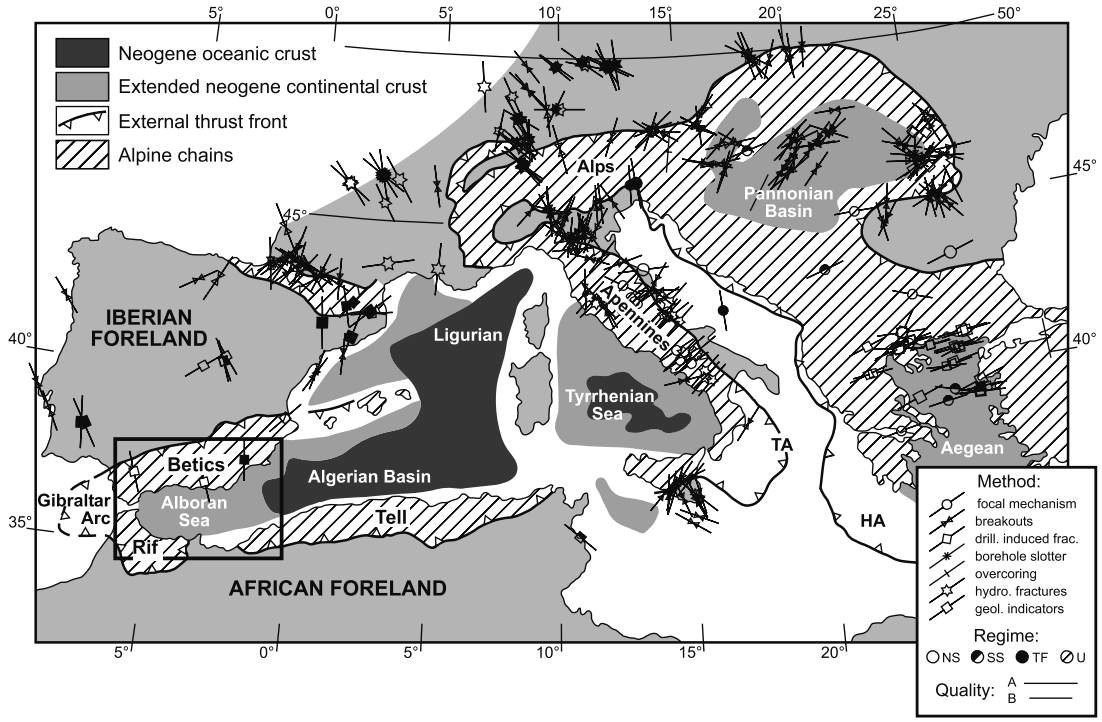

Figure 1. Tectonic scheme of the Alpine Chains in the Mediterranean Sea and the Neogene extensional basins [from *Comas et al.*, 1999]. Regional stress (S_{Hmax}) orientations are taken from the World Stress Map Project (2005 release) and completed from *Montone et al.* [2004] for the Italian peninsula, using the CASMI software [*Heidbach and Höhne*, 2004]. Only A and B quality data are plotted. The geology of the Gibraltar Arc region (GA), marked by a rectangle in the western Mediterranean, is shown in Figure 2. TA, Tyrrhenian Arc, and HA, Hellenic Arc.

the arc from the eastern Betics through the Alboran Sea to the Rif can be a source of stress perturbations.

2. Tectonic Setting

[4] The Betic (in southern Spain) and Rif (in northern Morocco) mountain chains form the westernmost Alpine orogenic belt in the Mediterranean. The Alboran Sea Basin, continuing to the east as the Algerian Basin, is located in the inner part of the Gibraltar Arc (Figure 2), which is one of the most arcuate orogenic belts in the world and is known to have formed during the Neogene in a general setting of Eurasian-African plate convergence [e.g., *Dewey*, 1988; *Platt and Vissers*, 1989; *Lonergan and White*, 1997; *Gueguen et al.*, 1998; *Comas et al.*, 1999; *Jolivet and Faccenna*, 2000; *Platt et al.*, 2003]. Kinematic reconstructions of relative motion between both plates reveal N-S convergence from middle Oligocene to late Miocene, and NW–SE convergence from the late Tortonian (~7 Ma) to the present [e.g., *Dewey et al.*, 1989; *Rosenbaum et al.*, 2002].

[5] The Gibraltar Arc was formed during the Neogene from simultaneous westward migration of the mountain front and late orogenic extension [e.g., *Dewey*, 1988; *Platt and Vissers*, 1989; *Gueguen et al.*, 1998; *Jolivet and Faccenna*, 2000]. Although it has been argued that late orogenic extension was superimposed on an earlier collisional orogen [e.g., *Platt and Vissers*, 1989; *García-Dueñas et al.*, 1992; *Platt et al.*, 2003; *Azañón and Crespo-Blanc*, 2000; *Martínez-Martínez and Azañon*, 1997; *Martínez-Martínez et al.*, 2002], the causes for extension are under debate [e.g., *Platt et al.*, 1998].

[6] The main geodynamic models proposed to explain the formation of the Gibraltar Arc can be summarized as (1) postorogenic collapse [e.g., *Platt and Vissers*, 1989; *Platt et al.*, 2003], (2) lithosphere delamination [*García-Dueñas et al.*, 1992; *Comas et al.*, 1992; *Seber et al.*, 1996a, 1996b; *Calvert et al.*, 2000], and (3) "rollback" of a subduction zone beneath the Alboran region [*Royden*, 1993; *Lonergan and White*, 1997]. There are many other subduction models that consider different geometries and directions for the subducting slab [*Morales et al.*, 1999; *Jolivet and Faccenna*, 2000; *Gutscher et al.*, 2002; *Faccenna et al.*, 2004]. Westward slab rollback accommodated by E-W lithosphere tearing along the southern margin of the Alboran Sea has also been proposed recently to explain collectively the strong curvature of the arc, the lithosphere slab seen in tomography [*Blanco and Spakman*, 1993; *Piromallo and Morelli*, 2003; *Spakman and Wortel*, 2004] and the limited N-S distance between the Eurasian and African plates throughout the Neogene [*Wortel and Spakman*, 2000; *Duggen et al.*, 2003, 2004; *Spakman and Wortel*, 2004].

[7] The Gibraltar Arc involves four pre-Neogene crustal domains (Figure 2): (1) the South Iberian and Maghrebian passive continental margins, corresponding to the External Zones of the Betics and Rif, respectively, and consisting of Mesozoic and Tertiary sedimentary rocks; (2) the Flysch Trough Units, mainly represented in the Rif and Tell regions, comprising sediments that originally occupied

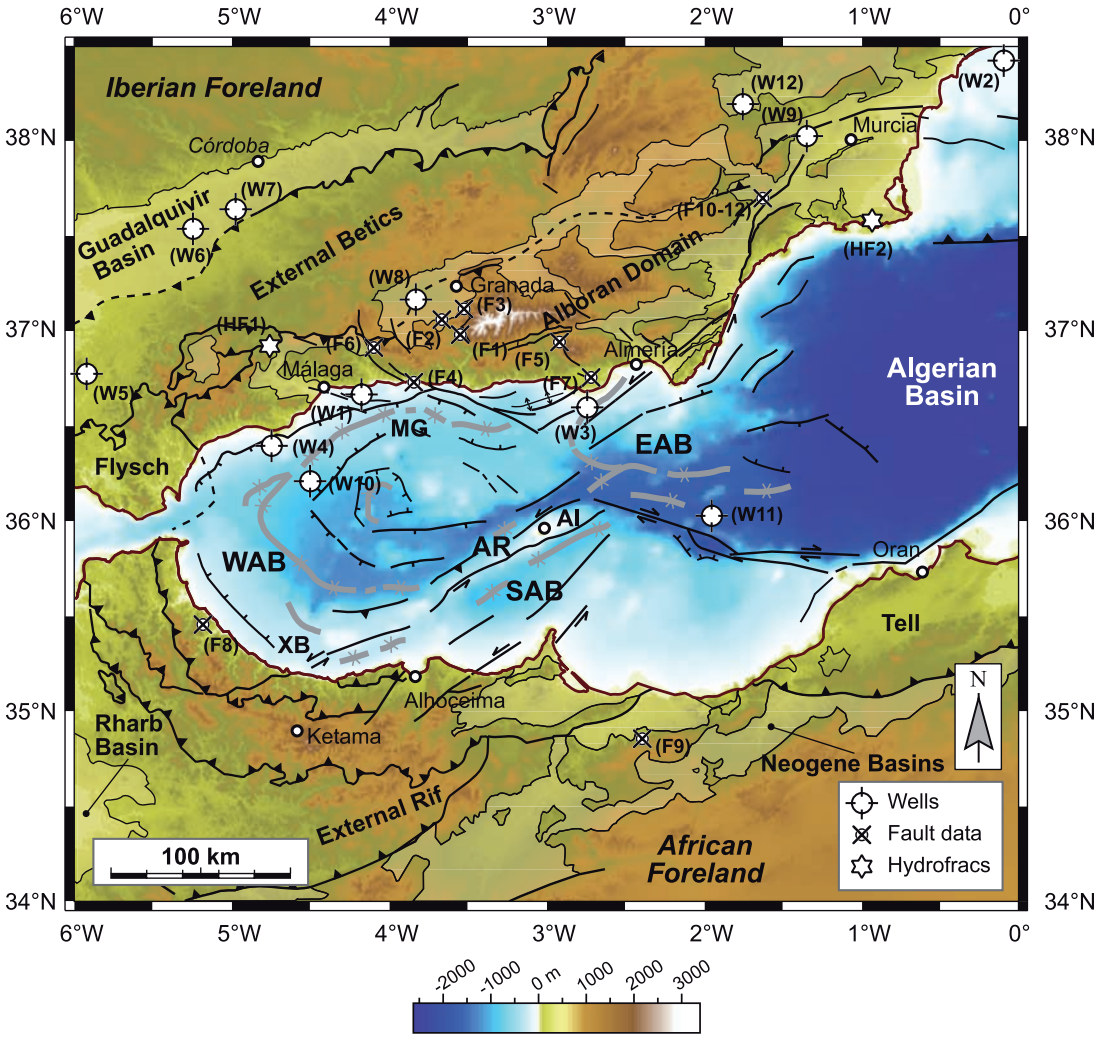

Figure 2. Geological domains and major tectonic features in the Gibraltar Arc (simplified from *Comas et al.* [1999]). Main subbasins in the Alboran Sea: WAB (West Alboran Basin), EAB (East Alboran Basin), and SAB (South Alboran Basin) and the location of the Algerian Basin (AB) are also indicated. Location of wells (W) used in the breakout analysis (Table 1), fault slip data (F) (Table 2), and hydraulic fracturing (HF) (Table 3) are included. Digital topography is built on the GTOPO30 (U.S. Geological Survey, USGS) global database combined with GEBCO 97 (IOC-IHO) global chart for the offshore region. AI, Alboran Island; AR, Alboran Ridge; MG, Malaga Graben; and XB, Xauen Bank.

oceanic troughs or very thin continental crust; and (3) the Alboran Crustal Domain: Paleozoic and Mesozoic rocks constituting the Betic-Rif Internal Zones and the floor of the Alboran Sea, which is composed of a thrust stack of three nappe complexes.

[8] The Alboran Sea Basin has three main subbasins (Figure 2): the West Alboran Basin (WAB), the East Alboran Basin (EAB), and the South Alboran Basin (SAB), separated by several ridges, seamounts and troughs that configure a complex seafloor morphology. The Alboran Ridge (AR) is the most outstanding feature, a NE–SW trending ridge bounded by large strike-slip faults [*Bourgois et al.*, 1992; *Campos et al.*, 1992; *Chalouan et al.*, 1997]. Major sedimentary accumulations are located in the WAB (>8 km thick, average water depth = 1000 m) defining an elongated depocenter of NNW to NNE trend that mimics the Gibraltar Arc curvature, turning to an E-W direction along the northern margin of the Alboran Sea [*Comas et al.*, 1992, 1999; *Watts et al.*, 1993; *Soto et al.*, 1996; *Chalouan et al.*, 1997]. The most ancient marine deposits (Aquitanian?-Burdigalian) overlie the metamorphic basement (the Alboran Domain) and consist of olistostromes containing clastic material and undercompacted shales [*Jurado and Comas*, 1992; *Comas et al.*, 1992, 1999]. Maximum sediment accumulations reach 3 km thick in the SAB and up to 2–3 km in the EAB (average water depth of 1200 m) at the transition toward the Algerian Basin (AB; average water depth of 2500 m) [*Comas et al.*, 1995; *Soto et al.*, 1996; *Mauffret et al.*, 2004].

[9] On land, the mountain ranges strike parallel to the shoreline with altitudes reaching over 3000 m in the Sierra Nevada mountain range (central and eastern Betics). Although topography reproduces the arcuate shape of the orogenic belt, the highest elevations are located

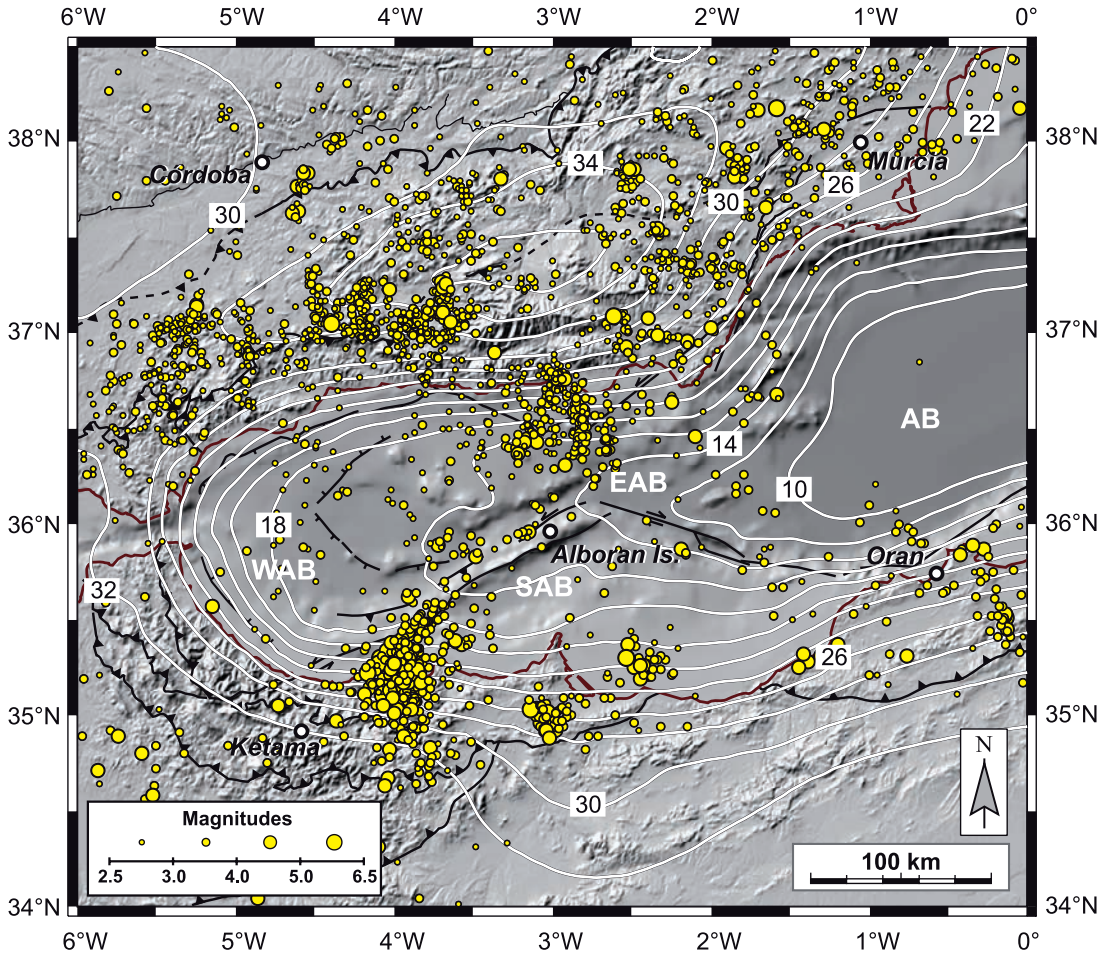

Figure 3. Crustal thickness and distribution of crustal seismic events ($M > 2.5$) in the Gibraltar Arc for the 1980–2006 period (taken from the USGS catalogue). Crustal thickness in the Alboran Sea is taken from *Torne et al.* [2000] and completed from *Ziegler and Dèzes* [2006] for the surrounding areas. AB, Algerian Basin; EAB, East Alboran Basin; SAB, South Alboran Basin; WAB, West Alboran Basin. Shaded relief map is constructed by combining Shuttle Radar Topography Mission (STRM) (NASA-USGS) and GEBCO 97 (Intergovernmental Oceanographic Commission–International Hydrographic Organization, IOC-IOH) global data sets. Geology is simplified from Figure 2.

on the eastern side of the Arc, far from the frontal part (Figure 2).

[10] Different space-geodetic models predict moderate NW–SE plate convergence between the Eurasian and African plates in the western Mediterranean (e.g., mean azimuth 134° and 115° with 5.1 and 4.6 mm yr^{-1} according to NUVEL-1A [*DeMets et al.*, 1994] and DEOS2K or IGSO2P09 [*Fernandes et al.*, 2003; *Nocquet and Calais*, 2004], respectively). On the basis of the geodetic observations available in southern Iberia and northern Africa, the different models depict a broad area of deformation with oblique convergence of Africa toward the NW with respect to fixed Eurasia [*DeMets et al.*, 1990, 1994; *Sella et al.*, 2002; *Kreemer and Holt*, 2001; *Nocquet et al.*, 2001; *Altamimi et al.*, 2002; *Fernandes et al.*, 2003; *Nocquet and Calais*, 2003, 2004]. Local GPS observations in the Rif and in the vicinity of the Strait of Gibraltar in the western Betics [e.g., *Reilly et al.*, 1992; *Nocquet and Calais*, 2004] suggest a lateral escape of the Gibraltar Arc domain southward and westward [*Fadil et al.*, 2006; *Stich et al.*, 2006]. Regarding NUVEL-1A [*DeMets et al.*, 1994], all the geodetic models indicate that Eurasia-Africa plate motion may be 40–50% slower (~4 mm yr^{-1} in the western Mediterranean) [*Altamimi et al.*, 2002; *Fernandes et al.*, 2003; *McClusky et al.*, 2003; *Nocquet and Calais*, 2003], although there is much uncertainty about the precise azimuth of the relative plate motion [e.g., *Nocquet and Calais*, 2004].

[11] Deep crustal seismic data and gravity modeling indicate that crustal structure is characterized by an arcuate bulge parallel to the Gibraltar Arc with an abrupt thinning from the Betics (maximum crustal thickness 37 km) and Rif (maximum crustal thickness 32 km) toward the Alboran Sea (Figure 3) [*Working Group for Deep Seismic Sounding in the Alboran Sea 1974*, 1978; *Torne et al.*, 1992; *Banda et al.*, 1993; *García-Dueñas et al.*, 1994; *Torne et al.*, 2000; *García-Castellanos et al.*, 2002; *Jiménez-Munt and Negredo*, 2003; *Ziegler and Dèzes*, 2006]. Crustal thinning occurs uniformly from the margins toward the Alboran Sea with the steepest gradient along the northern margin coin-

ciding with the shoreline [e.g., *Torne and Banda*, 1992; *Gallart et al.*, 1995; *Galindo-Zaldívar et al.*, 1997; *Torne et al.*, 2000]. The East Alboran Basin has thinned continental crust (<15 km), most probably becoming oceanic in nature toward the Algerian Basin [e.g., *Comas et al.*, 1995; *Mauffret et al.*, 2004].

[12] The lithosphere structure also shows an arcuate mantle bulge that mimics the Gibraltar Arc (lithosphere thickness of 130 km with 60–65 mW m^{-2}) and severe mantle thinning in the Alboran Sea (60–50 km with >90 mW m^{-2}) [*Polyak et al.*, 1996; *Torne et al.*, 2000], that is floored by an anomalous lithosphere mantle [*Working Group for Deep Seismic Sounding in the Alboran Sea 1974*, 1978; *Seber et al.*, 1996a, 1996b; *Calvert et al.*, 2000; *Gurría and Mezcua*, 2000; *Serrano et al.*, 2005]. There is also a distinctive pattern of crust and lithosphere thinning in the eastern Betics toward the Alboran Sea that may suggest crust-mantle decoupling during the most recent episodes of rifting [*Torne et al.*, 2000].

[13] The boundary between the African and Eurasian plates in the western Mediterranean is characterized by somewhat scattered seismicity [*Grimison and Chen*, 1986; *Udías and Buforn*, 1991; *Buforn et al.*, 1995; *López Casado et al.*, 2001; *Stich et al.*, 2003; *Buforn et al.*, 2004]. In fact, the distribution of crustal seismicity shows several seismic swarms, with abundant shallow depth earthquakes (Figure 3). It has been argued that the intermediate depth earthquakes in the area indicate a detached portion of lithosphere mantle, but it is not clear whether it is connected with the shallow, crustal seismicity [e.g., *Blanco and Spakman*, 1993; *Seber et al.*, 1996a, 1996b; *Mezcua and Rueda*, 1997; *Calvert et al.*, 2000; *Spakman and Wortel*, 2004]. In any case, focal depth distribution of earthquakes shows that most seismicity is in the upper, brittle crust (90% of the crustal seismicity is <15 km depth).

[14] Seismotectonic studies in the Gibraltar Arc indicate fault regimes that vary from normal to thrust faulting, with large strike-slip faults affecting sectors of the Betics and Rif [e.g., *Galindo-Zaldívar et al.*, 1993; *Buforn et al.*, 1995; *López Casado et al.*, 2001; *Stich et al.*, 2003]. These structures are thought to control most of the deformation in the southeastern Betics and East Alboran Basin during the Neogene [e.g., *Andreux et al.*, 1971; *Bousquet*, 1979; *Leblanc and Olivier*, 1984; *Weijermars*, 1987; *de Larouzière et al.*, 1988; *Montenat*, 1990; *Sanz de Galdeano*, 1990; *Cloetingh et al.*, 1992; *Montenat and Ott D'Estevou*, 1995; *Sanz de Galdeano et al.*, 1995; *Morel and Meghraoui*, 1996; *Alvarez-Marrón*, 1999]. Some segments of these strike-slip faults show evidence of active faulting during the Quaternary [e.g., *Keller et al.*, 1995; *Bell et al.*, 1997; *Reicherter and Reiss*, 2001; *Faulkner et al.*, 2003; *Martínez-Díaz and Hernández-Enrile*, 2004; *Masana et al.*, 2004; *Gràcia et al.*, 2006].

3. Characterization of the Present-Day Stress Field

[15] Four different types of data have been used to reconstruct present-day tectonic stress in the Gibraltar Arc: borehole breakouts, earthquake focal mechanisms, in situ stress measurements (hydraulic fracturing), and young geological data (fault slip).

3.1. Stress Orientation From Borehole Breakouts

[16] Borehole breakouts are stress induced zones of failure of the borehole wall resulting in enlargement and elongation of the wellbore cross section [e.g., *Bell and Gough*, 1979; *Cox*, 1982]. When a well is drilled the stress tends to concentrate at the borehole wall, surpassing rock strength and causing compressive failure of the wall [*Zoback et al.*, 1985; *Bell*, 1990]. In a vertical well, breakouts form symmetrically on both sides of the well at the azimuth of the minimum principal stress S_{hmin}.

[17] The data used to determine the orientation of breakouts usually come from a magnetically oriented four-arm caliper which is part of the dipmeter logging tool (such as Schlumberger's HDT and SHDT) commonly run in the hydrocarbon industry to obtain the strike and dip of bedding. Four-arm caliper tools record two perpendicular borehole diameters. Despite the relatively low sensitivity of this technique, with sufficient care it is possible to use four-arm caliper data to reliably determine breakout orientations [e.g., *Plumb and Hickman*, 1985; *Zoback and Zoback*, 1989; *Zoback et al.*, 2003]. Because most of the available data in the study region come from deep wells drilled during the 1980s, the records are paper logs. To identify zones of breakout and the orientation of the enlargement, we applied the criteria given by *Plumb and Hickman* [1985] with the additional constraint that the direction of hole enlargement not be parallel to the direction of well deviation. The mean borehole breakout azimuth and standard deviation for each well were determined using circular statistics described by *Mardia* [1972]. Appendix A describes the basic analytical procedure.

[18] A total of 12 data sets from wells with the four-arm caliper tool were selected throughout the Betics and Alboran Sea (Table 1 and Figure 2). In the Alboran Sea, we used commercial wells drilled mainly through Plio-Quaternary and late Miocene sediments (W-1 (Alborán A-1), W-3 (Andalucía A-1), W-4 (Andalucía G-1)), and the Ocean Drilling Program (ODP) Leg 161 holes (976B (W-10) and 977A (W-11)). W-10 well reaches the basement of the Alboran Sea Basin which consists of high-grade metamorphic rocks comparable with some of the rocks forming the Alboran Domain in the Betics [*Comas et al.*, 1999]. In the External Zones of the Betics two wells were selected (W-2 (Alicante A-1) and W-12 (Río Segura G-1)), both drilled through Mesozoic and Tertiary sedimentary rocks. The W-8 (Granada D-1) and W-9 (Murcia 4-1) wells were drilled through Neogene and Quaternary marine and continental deposits in the Granada and the Alhama-Fortuna basins, respectively, which are two of the main Neogene basins in the Betics. In the Guadalquivir foreland basin, to the NW of the Betics, we selected commercial wells W-6 (Córdoba A-7) and W-7 (Córdoba B-1). Both well logs consist of upper Miocene sedimentary rocks overlying the Paleozoic basement of the Hercynian massif (Iberian foreland). W-5 (Bética 18-1) was chosen to characterize the stress field on the western front of the Gibraltar Arc. It was drilled through a thick cover of Miocene to Triassic (allochthonous) clays and salts and also the Mesozoic autochthonous sediments (limestones and marls). As there is no well data available along the Rif Chain, other types of stress indicators, described in sections 3.2 and 3.4, have been used to define stress field in this region.

Table 1. Results of Wellbore Breakout Analysis Performed in the Region[a]

Station	Longitude	Latitude	S_{Hmax} ± SD	Stress Regime	Quality	Depth Interval of Breakouts, m	Total Length of Breakouts, m	Tool	Well Name
W-1	−4.21	36.63	32 ± 15	U	D	[2240, 2300]	15	SHDT	Alborán A-1
W-2	−0.03	38.46	57 ± 4	U	A	[1950, 2500]	350	HDT	Alicante A-1
W-3	−2.73	36.60	105 ± 12	U	B	[1400, 2150]	140	HDT	Andalucía A-1
W-4	−4.75	36.40	98 ± 4	U	A	[1300, 3100]	300	HDT	Andalucía G-1
W-5	−6.00	36.78	158 ± 19	U	C	[850, 1600]	220	HDT	Bética 18-1
W-6	−5.38	37.50	-	-	E	-	-	SHDT	Córdoba A-7
W-7	−5.27	37.56	38 ± 6	U	C	[650, 600]	35	SHDT	Córdoba B-1
W-8	−3.81	37.17	165 ± 22	U	D	[500, 770]	20	SHDT	Granada D-1
W-9	−1.35	38.02	7 ± 9	U	C	[770, 2160]	70	SHDT	Murcia 4-1
W-10	−4.31	36.21	40 ± 8	U	D	[700, 900]	15	HDT	ODP 976B
W-11	−1.96	36.03	38 ± 4	U	C	[420, 560]	45	HDT	ODP 977A
W-12	−1.75	38.20	36 ± 8	U	A	[2050, 3450]	365	HDT	Río Segura G-1

[a]Stress regime remains unknown (U) as there are no data available to constrain the relative stress magnitude in each hole. HDT, high-resolution dipmeter tool; SHDT, stratigraphic high-resolution dipmeter tool. The depth interval of breakouts is given in meters below sea level for offshore wells and below topographic surface for onshore wells.

[19] Zones of wellbore enlargement were recognized in 11 of the 12 selected wells to depths up to 3450 m. Mean orientation and standard deviation for each well were used to classify the quality of the wells following the borehole quality ranking criteria of *Zoback and Zoback* [1991]. Table 1 summarizes the results of breakout analysis performed in the selected wells, displaying depth interval with breakouts as well as the assigned quality resulting from the computed standard deviation and the total length of breakouts (three wells with A quality, 1 with B quality, four with C quality, three with D quality, and one with E quality). Because there is no constraint on stress magnitude (by means of leak-off tests, for example) the stress regime U (unknown) is given to every well.

[20] In the Alboran Sea two of the five wells used for this study (W-1 and W-10) do not have enough breakouts intervals to be considered reliable (or show washouts). In other words, these boreholes have only D quality data that are not reliable stress indicators. Although *de Larouzière et al.* [1999] characterized the tectonic stress at the ODP Site 976 (W-10) using downhole electrical images (FMS), these data are not considered reliable (D quality) because there is only a very short interval of the hole (∼15 m) with breakouts. The W-11 well displays a NE−SW constant S_{Hmax} attitude through the entire analyzed interval and has been classified as a C quality indicator since the total length of breakouts is <50 m. The W-3 and W-4 wells, on the northern shelf of the Alboran Sea, have a good quality ranking (B and A, respectively) and show a nearly E-W S_{Hmax} orientation (essentially parallel to the coastline). W-4, as well as some other wells, display local breakout rotations that can sometimes be correlated with discrete active fault zones affecting the local stress orientation [*Shamir and Zoback*, 1992; *Barton and Zoback*, 1994]. The significance of rotations in each particular hole was analyzed considering the available logging records and the lithologic descriptions and, consequently, the latter were included in the mean breakout orientation (see Appendix A for further details).

[21] In the External Betics, W-12 is a deep well (>5000 m) with a total length of breakouts of more than 300 m and hence it is a high-quality stress indicator (A quality). This well shows a NNE−SSW attitude for S_{Hmax}, which is fairly coherent with the orientation of S_{Hmax} at the nearby W-9 well. The latter is drilled in a Neogene basin and has a total length of 70 m with breakouts, so it is classified as a C quality indicator. W-8 is also drilled in a Neogene basin. It has been classified as a low-quality indicator (D quality) due to the presence of long washout intervals. W-2 is an offshore deep well (>2500 m) in the eastern Betics with high-quality stress data that show a NE−SW attitude for S_{Hmax}.

[22] From the well data along the Guadalquivir Basin, only W-7 has some intervals with breakouts and a total length <40 m (C quality) inferring a NE-SW trend for S_{Hmax}. W-6 has a poor caliper data record with many washouts and no breakouts.

[23] The W-5 well, located on the western front of the Gibraltar Arc, displays many intervals where the tool orientation gets locked at depths over 1600 m and is thus not suitable for analysis. Hence, in this well we have only analyzed breakout orientations at depths up to 1600 m. For this interval, as was remarked above, there is a considerable amount of interbedded salt layers that operate as decoupling levels and cause sudden breakout rotations [*Evans*, 1989].

3.2. Stress Information From Fault Slip Data

[24] Kinematic data from selected faults have been compiled as part of our stress field characterization along the Gibraltar Arc (Table 2, and Figure 2 for location). The stress ellipsoids inverted by other authors for active faults have also been taken into account. Only currently active structures or faults that can be demonstrated to be active during the past 1.65 Ma (i.e., Quaternary) are considered in this study. In order to obtain a more definitive stress map, a lower quality label has been assigned to those faults thought to be active during the early Quaternary.

[25] To determine the present-day stress field, at least 15 measurements of fault strike and dip and rake of the striae were taken at each station and the stress tensor was calculated by the direct inversion method as described by *Angelier and Goguel* [1979]. Results were tested using other stress inversion methods. The dihedra calculation method of *Angelier and Mechler* [1977] for the analyzed data set agrees with the above direct inversion results. P, B, and T axes were also calculated following *Turner* [1953]. These axes show a relatively good match with the three principal stress axes derived from the dihedra calculation and the direct inversion methods.

Table 2. Fault Slip Data in Quaternary Age Faults Used for Stress Inversion[a]

Station	Longitude	Latitude	P Axis (σ_1)	B Axis (σ_2)	T Axis (σ_3)	S_{Hmax}	Stress Regime	Quality	Axial Ratio	Source
F-1	−3.56	37.00	79/183	07/311	08/042	313	NF	A	0.50	1
F-2	−3.66	37.07	86/211	00/301	04/031	303	NF	A	0.48	1
F-3	−3.53	37.13	67/019	17/157	14/252	159	NF	C	0.52	1
F-4	−3.80	36.76	67/263	22/094	04/003	96	NF	B	0.01	1
F-5	−2.89	36.90	70/048	02/143	20/234	145	NF	A	0.49	1
F-6	−4.10	36.92	44/008	46/188	00/098	280	NS	A	0.25	2
F-7	−2.72	36.75	81/144	08/297	04/028	297	NF	A	0.10	3
F-8	−5.18	35.32	64/073	25/268	06/175	268	NF	A	0.45	4
F-9	−2.40	34.85	01/156	65/068	25/246	156	SS	A	0.16	5
F-10	−1.66	37.70	08/355	04/086	80/205	355	TF	A	0.14	6
F-11	−1.65	37.70	09/353	44/092	44/254	353	TS	A	0.24	6
F-12	−1.63	37.71	01/172	02/262	87/040	172	TF	A	0.16	6

[a]Sources are 1, own data; 2, *Galindo-Zaldívar et al.* [1999]; 3, *Marín-Lechado et al.* [2005]; 4, *Saji and Chalouan* [1995]; 5, *Aït-Brahim et al.* [2002]; and 6, *Martínez-Díaz* [2002]. NF, normal faulting; NS, predominantly normal faulting with strike-slip component; SS, strike-slip faulting; TS, predominantly thrust faulting with strike-slip component; TS, thrust faulting.

[26] Although faults are widely used to estimate stress in deformed rocks [e.g., *Angelier*, 1979; *Armijo et al.*, 1982; *Fry*, 2001], we are aware that conversion of slip vectors to stress orientations requires a number of not always well-constrained assumptions. First, because it is under discussion whether fault slip analysis results could be treated in terms of stress, strain or strain rate [e.g., *Marrett and Allmendinger*, 1990; *Twiss and Unruh*, 1998]. Second, because intermittent fault slip, asynchronous slip along the fault [e.g., *Gutscher et al.*, 1996] or heterogeneous stress distributions in structurally complex areas [e.g., *Mitra*, 1987] may lead to errors in stress calculations. However, stress inversion from fault slip data is commonly carried out by structural geologists. The inversion methods we have used are demonstrated to be valid for this sort of studies [e.g., *Fry*, 2001]. Despite these notes of caution, the results appear to be reliable since they match the S_{Hmax} orientation inferred from other types of stress indicators.

[27] The data we use include high-angle normal faults in the Granada Basin (e.g., F-1 and F-2 stations) in the central Betics. They correspond to SW dipping faults affecting recent alluvial fans with evidence of associated seismic activity [e.g., *Alfaro et al.*, 2001]. F-3 corresponds to early Quaternary high-angle normal faults that configure the western slope of the Sierra Nevada mountain range, but it is not clear whether these faults are seismically active at present. F-3 was therefore classified as a C quality stress indicator. At these stations, stress inversion shows a NW–SE orientation of S_{Hmax}.

[28] With the same criteria we have also considered the stress analysis carried out by *Galindo-Zaldívar et al.* [1999] in the Zafarraya fault (F-6 station). This is an active normal fault located west of the Granada Basin dipping to the north with roughly E-W orientation. It is known to have been active in historic times, causing one of the biggest earthquakes in the region in 1884 at Arenas del Rey ($M_w \approx 6.8$) [*Udías and Muñoz*, 1979; *Reicherter et al.*, 2003]. S_{Hmax} displays a WNW–ESE attitude in this region.

[29] Along the North Alboran margin F-4, F-5, and F-7 correspond to high-angle normal faults dipping to the SW and running oblique to the present coastline. F-4 includes measurements from a normal fault system that appears to continue offshore. The last fault slip is considered to have occurred during the early Pleistocene, on the basis of the geometrical relationships with alluvial fan deposits and radiometric data [*Soto and Manzano*, 2002], so we have assigned B quality to this stress indicator. S_{Hmax} at station F-4 shows a 96° azimuth. F-5 corresponds to recent fault structures located on the western slope of Sierra de Gádor. These structures were previously described by some authors [e.g., *Martínez-Díaz and Hernández-Enrile*, 2004] as high-angle normal faults with NW–SE attitude and SW dipping affecting Quaternary colluvial deposits. The F-7 station includes normal faults analyzed by *Marín-Lechado et al.* [2005] in the Campo de Dalías region. These structures are located near the coastline and affect Quaternary deposits. In this region, S_{Hmax} varies from WNW–ESE orientation at F-7 to NW–SE at F-5.

[30] Interpretation of kinematic data from microstructural and mesostructural observations carried out by *Martínez-Díaz* [2002] in the eastern Betics provides stress inversion solutions for the Alhama de Murcia fault system (stations F-10 to F-12). This is a reverse fault zone, with minor left-lateral strike-slip motion, that evidences recent Quaternary activity [*Masana et al.*, 2004]. Alluvial fans associated to fault scarps and the local drainage network are deformed by fault activity. Stress inversion data suggest a N-S attitude of S_{Hmax} in this region (varies from 172° to 175°).

[31] We have also compiled fault slip data from stations F-8 and F-9 in two regions of the Rif. F-8 corresponds to the stress inversion performed by *Saji and Chalouan* [1995] for a normal fault system in the Tetouan Basin (western Rif) that results in a W–E attitude of S_{Hmax}. F-9 includes the stress analysis carried out by *Aït-Brahim et al.* [2002] in a N-S normal fault system affecting Quaternary terraces in the Oujda region (east of the Rif). Stress inversion in this area suggests a NNW–SSE orientation of S_{Hmax}.

[32] It should be also noted that at some stations (e.g., F-4 and F-7) the stress ellipsoid axial ratio is significantly low (i.e., $\sigma_1 \approx \sigma_2$), making possible some horizontal principal stress axes permutation in reverse faulting environments.

Table 3. Data Set of Hydraulic Fracturing Stations Corrected for Magnetic Declination

Station	Longitude	Latitude	$S_{Hmax} \pm SD$	Stress Regime[a]	Quality	Depth, m
HF-1	−4.73	36.92	112 ± 4	U	A	[65, 450]
HF-2	−0.92	37.59	175 ± 5	U	B	[124, 185]

[a]U, unknown stress regime.

Table 4. Maximum Horizontal Stress Determination by Average P Axis From Earthquake Single-Event Solutions[a]

Station	Longitude	Latitude	S_{Hmax}	Stress Regime	Quality	Number of Events	Depth Interval	Average Depth, km	Source	Reference[b]
FM-1	−3.24	36.37	176	SS	A	6	[6, 16]	11	IAG	1–6
FM-2	−3.90	35.15	150	SS	A	7	[10, 16]	12.6	IAG	7–13
FM-3	−4.06	35.19	341	SS	A	4	[6, 16]	12	IAG	14–17
FM-4	−3.84	34.87	146	NF	B	3	[4, 6]	5.3	IAG	18–20
FM-5	−4.08	35.05	332	SS	A	5	[6, 22]	13.6	IAG	21–25
FM-6	−3.61	35.67	11	NS	B	6	[2, 6]	3.7	IAG	26–31
FM-7	−3.79	37.11	322	NF	A	5	[6, 16]	11	IAG	32–36
FM-8	−4.20	37.25	302	SS	B	3	[12, 14]	12.7	IAG	37–39
FM-9	−3.8	37.73	327	TF	B	2	[2, 2.5]	2.25	IAG[c]	40–41
FM-10	−1.82	37.85	323	NS	A	5	[6, 10]	6.8	IAG	42–46
FM-11	−3.00	34.94	145	SS	A	4	[6, 12]	9.5	IAG	47–50
FM-12	−3.90	35.55	176	SS	A	5	[8, 18]	12	IAG	51–55

[a]See single-event grouping in Figure 4. A quality results are from events located in close geographic proximity (at least one event $M_w \geq 4.0$, other events $M_w \geq 3.0$). B quality results are from average of two or three well-constrained single-event solutions ($M_w \geq 3.5$ by moment tensor inversion). IAG, Instituto Andaluz de Geofísica; NF, normal faulting; NS, predominantly normal faulting with strike-slip component; SS, strike-slip faulting; TS, predominantly thrust faulting with strike-slip component; TS, thrust faulting.
[b]Reference number of the single-event solution listed in Table B1.
[c]From *Sánchez-Gómez and Torcal* [2002].

3.3. Stress Orientation From Hydraulic Fracturing

[33] Hydraulic fracturing in boreholes can be used to estimate the orientation of S_{Hmax} and the magnitude of the least principal stress (usually S_{hmin}) at different depths in the upper crust [e.g., *Haimson and Fairhurst*, 1967]. In a vertical hole, hydraulic fractures are expected to be vertical at the azimuth of the maximum horizontal stress. The mean orientation of hydraulic fractures is available from stations HF-1 and HF-2 (Table 3, see Figure 2 for location). At the HF-1 site, two wells were drilled to a depth of over 450 m and a set of 9 measurements taken in each at a range of depths from 65 m to 450 m. An average of the hydraulic induced fractures for both wells was computed, resulting in a N110°E strike of the S_{Hmax}. The well drilled at the HF-2 site has a maximum depth of 205 m and 10 measurements were taken at depths between 124 m and 185 m. The resulting mean orientation of S_{Hmax} is N174°E.

3.4. Stress Information From Focal Mechanisms

[34] The Instituto Andaluz de Geofísica (IAG) and Instituto Geográfico Nacional (IGN) maintain two permanent seismic networks in SE Spain and northern Morocco. Most of the data gathered for this study belong to the IAG Regional Moment Tensor Project catalogue, which is publicly available (http://www.ugr.es/∼iag/tensor/). The IGN database and some other published data are used to com-

Table 5. Maximum Horizontal Stress From Well-Constrained Single-Event Solutions by Moment Tensor Inversion[a]

Station	Longitude	Latitude	P Axis σ_1	B Axis σ_2	T Axis σ_3	S_{Hmax}	Stress Regime	Quality	M_w	Depth, km	Source	Reference[b]
FM-13	−3.55	35.67	03/009	67/106	12/077	011	SS	B	4.8	4	IAG	56
FM-14	−3.55	35.95	40/357	46/145	16/253	345	SS	C	3.8	14	IAG	57
FM-15	−2.74	36.21	51/303	38/106	08/202	294	NS	C	3.9	6	IAG	58
FM-16	−3.92	35.18	19/334	71/131	04/242	334	SS	B	4.5	14	IAG	59
FM-17	−3.86	35.05	21/330	69/159	03/061	153	SS	B	5.2	10	IAG	60
FM-18	−4.15	35.00	34/334	53/182	14/073	165	SS	B	4.5	10	IAG	61
FM-19	−4.05	34.92	70/331	20/154	01/063	156	NF	B	4.9	6	IAG	62
FM-20	−4.00	35.14	25/329	65/148	01/239	351	SS	B	6.3	14	IAG	63
FM-21	−2.55	37.09	78/262	01/167	12/077	169	NF	B	4.7	10	IAG	64
FM-22	−1.79	37.01	11/335	55/081	33/237	337	SS	C	3.9	8	IAG	65
FM-23	−2.65	37.53	81/015	08/168	04/259	170	NF	C	4.1	8	IAG	66
FM-24	−5.56	36.90	06/305	05/035	83/165	307	TF	C	3.5	6	IAG	67
FM-25	−4.70	37.74	06/283	84/104	00/013	285	SS	C	4.2	12	IAG	68
FM-26	−1.57	36.68	15/327	18/062	66/201	328	TF	C	3.8	3	IGN	69
FM-27	−1.84	37.90	43/325	46/158	07/061	153	NS	B	5.0	8	IAG	70
FM-28	−1.78	37.88	23/359	62/142	15/263	001	SS	B	4.8	10	IAG	71
FM-29	−0.03	35.40	00/324	04/234	86/058	326	TF	B	5.7	4	(1)	72
FM-30	−2.53	35.27	23/131	67/303	03/040	135	SS	B	4.8	30	(1)	73
FM-31	−1.49	38.11	33/360	57/185	02/092	184	SS	B	4.8	6	IAG	74
FM-32	−1.69	38.18	30/187	55/041	16/287	019	SS	C	3.8	6	IAG	75
FM-33	−1.77	37.66	16/135	10/228	71/349	138	TF	C	3.7	4	IAG	76
FM-34	−0.43	35.89	11/329	26/064	61/217	335	TF	B	5.1	5	(2)	77
FM-35	−0.10	35.50	33/162	54/316	13/064	158	SS	C	4.2	16	(3)	78
FM-36	−5.27	37.16	17/026	29/285	5/142	028	TF	C	4.1	4	IAG	79
FM-37	−1.28	35.32	26/307	10/213	62/103	309	TF	B	5.7	8	(4)	80
FM-38	−5.17	35.57	80/179	01/083	10/353	085	NF	C	4.3	10	IAG	81

[a]B quality for $M_w \geq 4.5$ and C quality for $M_w \geq 2.5$ events. Sources are 1, *Bezzeghoud and Buforn* [1999]; 2, *McKenzie* [1972]; 3, *Coca and Buforn* [1994]; and 4, *Yelles et al.* [2004]. IAG, Instituto Andaluz de Geofísica; IGN, Instituto Geográfico Nacional; NF, normal faulting; NS, predominantly normal faulting with strike-slip component; SS, strike-slip faulting; TS, predominantly thrust faulting with strike-slip component; TS, thrust faulting.
[b]Reference number of the single-event solution listed in Table B1.

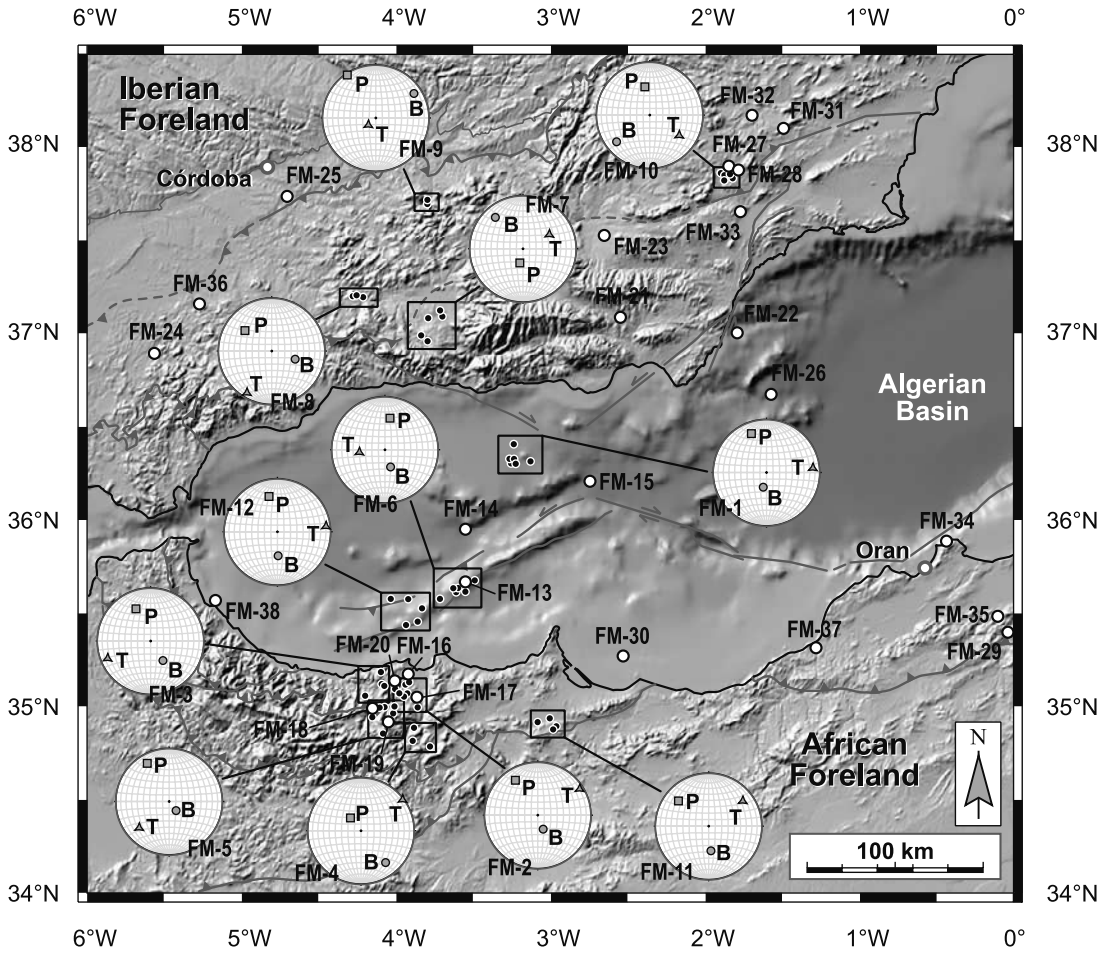

Figure 4. Location of the earthquake focal plane mechanisms used in this study. Focal mechanisms are shown in Figure B1 (Appendix B). Single-event solutions are represented with large solid circles (Table 5). Grouping of events for average P axis estimation are indicated with small solid circles inside a box (Table 4). Mean P, T, and B axes projection of the events grouped are plotted in lower hemisphere, equal-area projection. Geology is simplified from Figure 2.

plete this information locally in regions with poor azimuth coverage lying on the edge of the IAG network (e.g., western Algeria).

[35] The IAG has a permanent network of 9 short-period stations and 10–12 broadband stations operating in SE Spain. Most of these stations are located in the Iberian Peninsula, but a few are operated in North Africa. All waveforms have been available in digital format since 1992, and focal mechanism data are considered to be quite reliable to constrain the regional stress field as they have been inverted for a deviatoric moment tensor using complete seismograms recorded at local-to-regional distances (<1000 km) including the full waveform of P, S, Love, and Rayleigh waves. The moment tensor inversion method is detailed by *Stich et al.* [2003]. Well-constrained single-event solutions ($M_w \geq 4.5$) from first motions and other methods (moment tensor waveform modeling or inversion) or the average of several well constrained composites ($M_w \geq 2.0$) have been also included to complete the database locally (see sources in Tables 4 and 5).

[36] A total of 38 stress indicators were derived from the focal mechanism data (Tables 4 and 5 and Figure 4), which are classified according to how well the mechanisms are constrained and the source of the data. Stress indicators include the average P axis of four or more single-event solutions in close geographic proximity (Table 4; see grouping criteria shown in Figure 4) and also well-constrained single-event solutions (Table 5) both ranging from A to C in quality ranking. We selected earthquakes with $M_w \geq 2.5$. $M_w \geq 3.5$ seismic events were classified as A and B quality data sets, since their good waveform match at all stations suggests that both the inverted mechanisms and the correction of propagation effects are accurate for these events. Earthquakes with magnitudes ranging from 2.5 to 3.5 were included in our data set as C quality indicators. Smaller events are numerous in the area and while valuable for general seismotectonic interpretations, their recordings are often affected by noise and the quality of the focal mechanism are quite poor.

[37] Throughout North Africa most focal mechanism data correspond to strike-slip faulting, turning into reverse type to the east (Figure 4) [e.g., *Meghraoui et al.*, 2004; *Déverchère et al.*, 2005]. In the Alboran Sea and eastern Betics, focal mechanisms also correspond to strike-slip

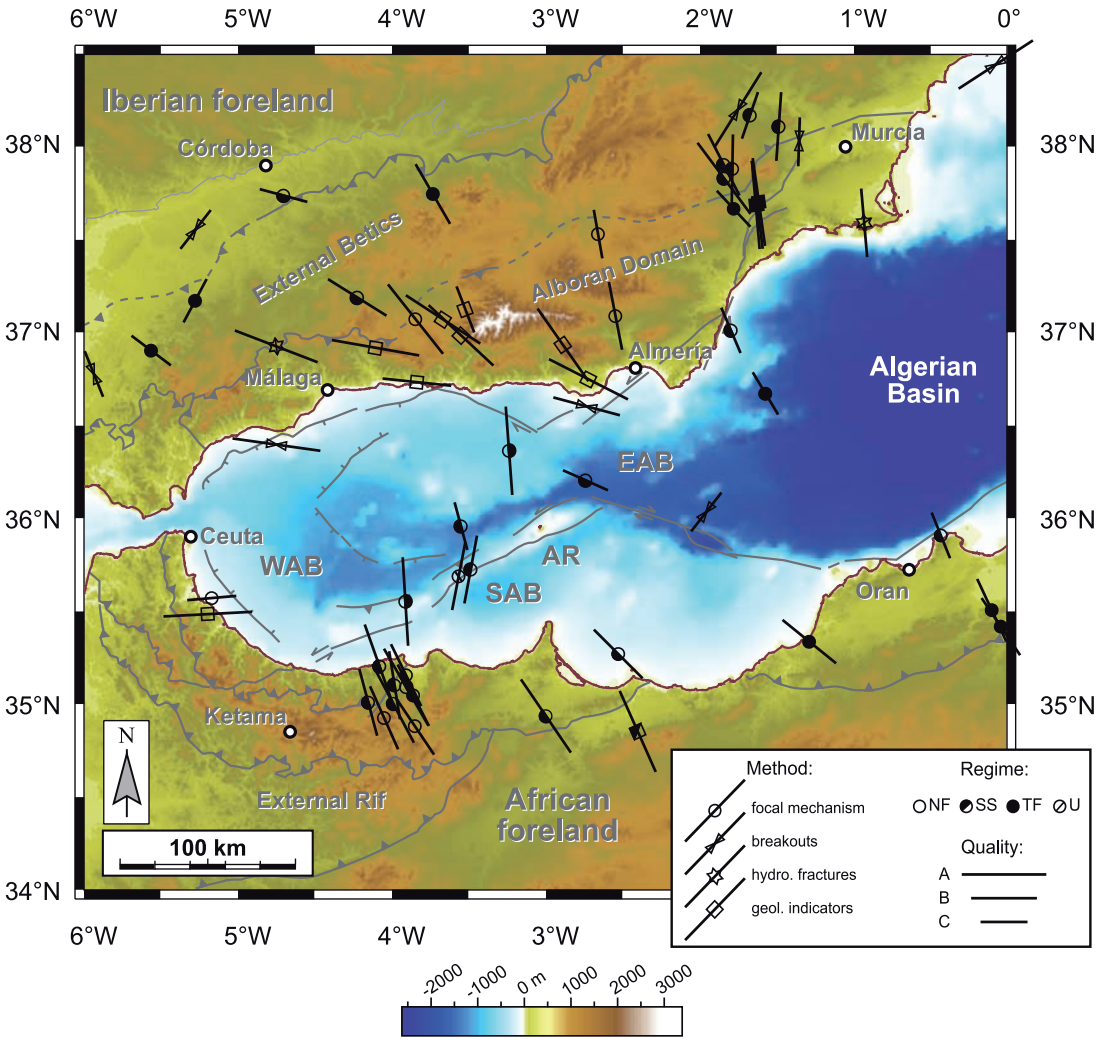

Figure 5. Maximum horizontal compressive stress (S_{Hmax}) map of the Gibraltar Arc from focal mechanisms, breakouts, hydraulic fracturing, and fault slip data. AR, Alboran Ridge; EAB, East Alboran Basin; SAB, South Alboran Basin; WAB, West Alboran Basin. Geology is simplified from Figure 2.

faults. In the central Betics the focal mechanisms indicate normal faulting. To the NW, toward the Guadalquivir Basin, strike-slip and thrust faulting occurs. Appendix B gives a more detailed description of focal mechanisms distribution in the Gibraltar Arc. The relatively complex stress pattern indicated by the focal mechanism data agree with the stress field inferred from the other indicators as will be described next.

3.5. Present-Day Stress Field

[38] On the basis of the stress indicators described in sections 3.1 to 3.4, we present the Gibraltar Arc stress map (Figure 5) that draws a complex stress pattern in the region. Overall, the direction of maximum horizontal compression (S_{Hmax}) displays a NNW–SSE attitude throughout North Africa, but near the Strait of Gibraltar it runs E-W. In the central Alboran Sea (along the Alboran Ridge and to the north) the direction of maximum horizontal stress shows a N-S attitude. In the Betics the stress pattern becomes more complex and three different stress provinces can be distinguished: (1) the North Alboran margin, where both onshore and offshore stress indicators evidence that S_{Hmax} runs subparallel to the margin along a narrow zone centered on the coastline; (2) the central Betics, where stress indicators suggest a roughly NW–SE orientation; and (3) the eastern Betics, where S_{Hmax} reveals a nearly constant N-S orientation with some minor local deviations. The Guadalquivir Basin and the frontal thrust of the External Betics in the NW region show a complex stress pattern with low-quality indicators that seem to be roughly orientated NW–SE, with some local deviations that point out the tectonic complexities of the area (Figure 5). There is a lack of data for the East Alboran Basin and its transition to the Algerian Basin and also for the Strait of Gibraltar area. These areas need to be completed with new data in further research.

4. Discussion

[39] The stress pattern described in section 3.5 suggests that the stress field in the Gibraltar Arc is mostly enforced by the NE–SW plate convergence between Africa and Eurasia. Nonetheless, it is observed that some deviations

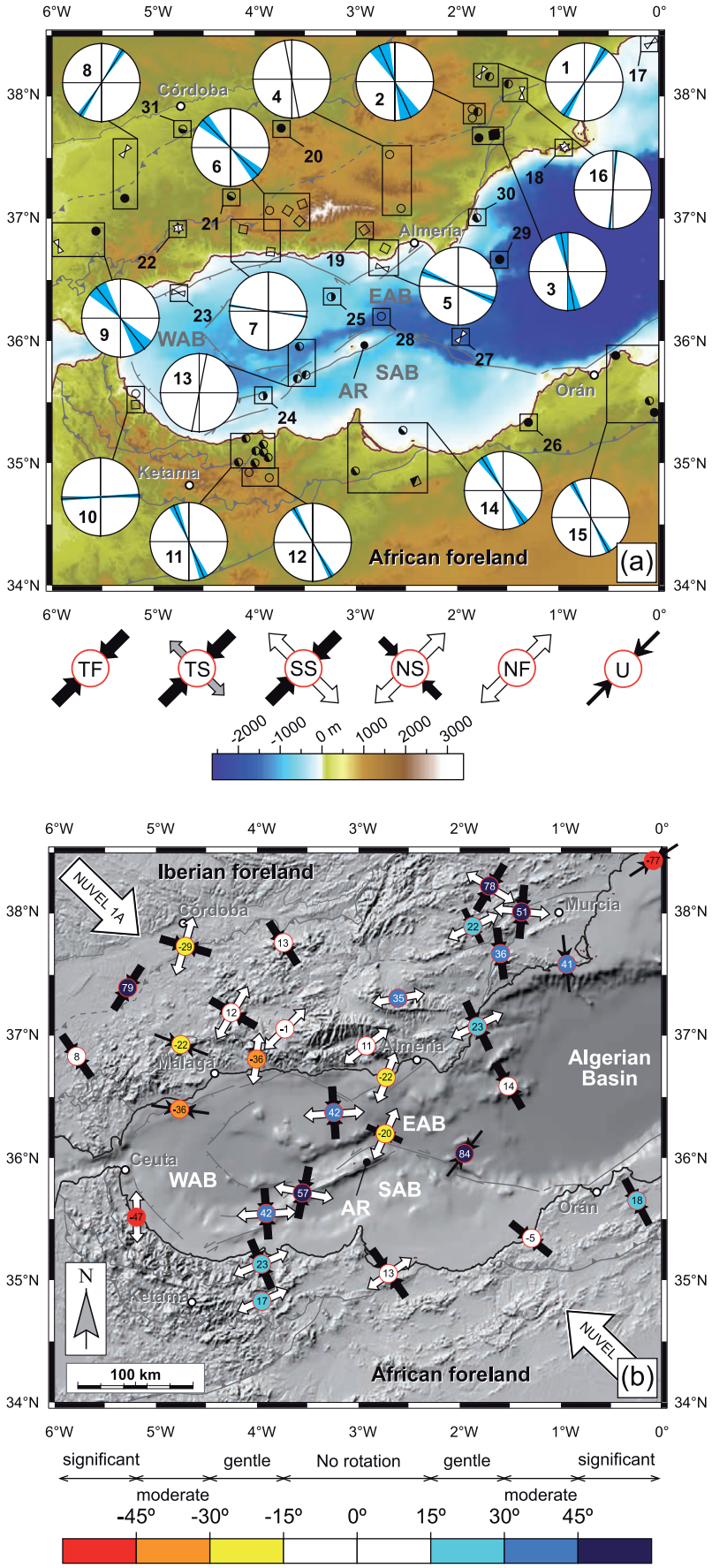
6°W
5°W
4°W
3°W
2°W
1°W
0°
38°N
37°N
36°N
35°N
34°N
Córdoba
Almería
Orán
Ketama
EAB
WAB
SAB
AR
African foreland
(a)
TF
TS
SS
NS
NF
U
-2000
-1000
0 m
1000
2000
3000
Iberian foreland
NUVEL 1A
Murcia
Málaga
Ceuta
Algerian Basin
N
100 km
NUVEL
(b)
significant
gentle
No rotation
gentle
significant
moderate
moderate
-45º
-30º
-15º
0º
15º
30º
45º

Figure 6

Table 6. Grouping of Stress Data Used to Elaborate the Synthetic Stress Map of Figure 6a[a]

Indicator	S_{Hmax}	SD	Rotation γ Angle[b]	Regimen	Stress Data
1	32	7	78	NF	W-12, FM-32
2	156	16	22	NS	FM-10, FM-27, FM-28
3	170	10	36	TF	FM-33, F-10, F-11, F-12
4	169	-	35	NF	FM-21, FM-23
5	112	6	−22	NF	F-7, W-3
6	135	11	−1	NF	F-1, F-2, F-3, FM-7
7	98	2	−36	NF	F-4, F-6
8	33	5	79	TF	FM-36, W-7
9	142	16	8	TF	FM-24, W-5
10	87	1	−47	NF	F-8, FM-38
11	157	7	23	SS	FM-2, FM-3, FM-5, FM-16, FM-17, FM-18, FM-20
12	151	5	17	NF	FM-4, FM-19
13	11	-	57	SS	FM-13, FM-6
14	147	8	13	SS	FM-30, FM-11, F-9
15	152	5	18	TF	FM-34, FM-35, FM-29
16	5	1	51	SS	W-9, FM-31
17	57	4	−77	U	W-2
18	175	5	41	U	HF-2
19	145	9	11	NF	F-5
20	327	-	13	TF	FM-9
21	302	-	12	SS	FM-8
22	112	4	−22	U	HF-1
23	98	4	−36	U	W-4
24	176	-	42	SS	FM-12
25	176	-	42	SS	FM-1
26	309	-	−5	TF	FM-37
27	38	4	84	U	W-11
28	294	-	−20	NS	FM-15
29	328	-	14	TF	FM-26
30	337	-	23	SS	FM-22
31	285	-	−29	SS	FM-25

[a]Stress rotations are plotted in Figures 6b and 8b.
[b]Rotation is given as the angle (γ) between S_{Hmax} and the mean orientation of NUVEL-1A in the region: 134° ± 15° at 4°W, 36°N [*DeMets et al.*, 1994].

of different sense and magnitude occur apart from the plate convergence direction. To better assess the role of these deviations, the Gibraltar Arc stress map was analyzed by grouping stress indicators in a close geographic position, taking into account the stress regime and the geological information (e.g., indicators within the same geological domain). The grouping is shown in Figure 6a and the statistical results per site (average value and standard deviation) are detailed in Table 6.

[40] We consider the orientation of S_{Hmax} as regards the relative plate motion defined by the NUVEL-1A model [*DeMets et al.*, 1994]. Following this geodetic model, the plate convergence vector for a point centered in the region (4°W, 36°N) has a 134° azimuth with an associated standard deviation of ±15°. Considering this as a mean value of the regional stresses for the Gibraltar Arc (computed azimuths with this model vary between 145° and 120°), we estimate the deviation of S_{Hmax} apart from NUVEL-1A (Table 6). These angles appear as circled numbers in Figure 6b. Positive and negative values refer to clockwise and anticlockwise rotations, respectively, of S_{Hmax} with respect to NUVEL-1A.

[41] According to the WSM criteria [*Zoback*, 1992] the error associated with S_{Hmax} varies depending on the stress indicator quality: up to ±15° for A and B quality indicators and up to ±25° for C quality indicators. Regarding these uncertainties associated to each stress indicator and the intrinsic error of NUVEL-1A (±15°), we have developed a semiquantitative scale to verify the significance of the deviations observed in the region. In this manner, ≤15° deviations are not considered stress rotations, 15°–30° deviations are defined as gentle stress rotations, 30°–45° deviations are moderate rotations and >45° deviations are significant rotations with respect to the plate convergence. Figure 6b uses a color scale to describe the magnitude of the stress rotations in the region.

Figure 6. Generalized stress map of the Gibraltar Arc resulting from grouping different types of stress indicators in a close geographic position. (a) Grouped stress indicators included in a rectangular box with a rose diagram showing mean orientation of S_{Hmax} and standard deviation (see Table 6). Stress indicator symbols are as in Figure 5. (b) Local stress regime and amount of rotation of S_{Hmax} with respect to the mean orientation of Africa-Eurasia plate convergence. Large arrows correspond to the Africa-Eurasia relative motion according to NUVEL-1A (134°) [*DeMets et al.*, 1994]. Positive and negative values at the center of the arrow indicate clockwise and anticlockwise rotations, respectively (following the criteria of *Sonder* [1990]). The significance of rotations is classified using a color scale. NF, normal faulting; NS, predominantly normal faulting with strike-slip component; SS, strike-slip faulting; TS, predominantly thrust faulting with strike-slip component; TS, thrust faulting; U, unknown stress regime; AR, Alboran Ridge; EAB, East Alboran Basin; SAB, South Alboran Basin; WAB, West Alboran Basin. Geology is simplified from Figure 2.

[42] On the basis of these criteria, stress orientations throughout North Africa (from 0° to 5°W) are fairly consistent with the stress field imposed by plate motion, with gentle clockwise rotations or none at all in the Alhoceima region (<25°; 4°W, 35°N) and western Tell region (−5° to 18°; at 0°−2°W, 35.5°N). Only one significant anticlockwise stress rotation was identified at the westernmost end of the South Alboran margin, in the Rif (−47° in the Tetouan basin). high-quality data in the Alboran Sea tend to concentrate around the Alboran Ridge where moderate-to-significant clockwise rotations (>30°) are found.

[43] Onshore and offshore indicators close to the northern coastline of the Alboran Sea show gentle-to-moderate anticlockwise rotations, apparently increasing westward, from Almería (−22°; 2.75°W, 36.5°N) to west of Málaga (−36°; 4.75°W, 36.5°N). North of the Iberian shoreline, in the central Betics, stress indicators run subparallel to plate convergence (rotations <15°; from −1° to 11°). Therefore E-W orientations of S_{Hmax} seem to be constrained to a narrow band centered on the North Alboran margin. East of 3°W (eastern Betics) S_{Hmax} shows a N-S attitude, resulting in clockwise rotations ranging from 22° to 78°, thus indicating a differential rotation within the same stress province. Stress orientations described in the eastern Betics and along the North Alboran margin agree with the GPS data recently presented by *Stich et al.* [2006].

[44] Data from the Guadalquivir foreland basin and the frontal thrust of the External Betics seem to agree with plate convergence (<15° rotations), but locally sudden clockwise and anticlockwise stress rotations occur (e.g., groups no. 8 and 31). Thus more accurate stress data are required to better describe stress field in this region.

4.1. Sources of Stress Rotation

[45] As many authors have demonstrated, second-order stress patterns can be related to flexural stresses and/or lateral density or strength contrasts [e.g., *Stein et al.*, 1989; *Sonder*, 1990; *Zoback et al.*, 1989; *Zoback*, 1992]. Locally, nonplanar fault geometries or fault tips can also produce stress perturbations [e.g., *Pollard and Segall*, 1987]. Following the scheme proposed by *Sonder* [1990] for stress rotations, we explore moderate to significant stress rotations observed in the Gibraltar Arc. The angle in the horizontal plane between the regional stress (S_{HRmax}) and the local source of stress (S_{HLmax}) causing a rotation to the resultant stress (S_{Hmax}) is defined by the θ angle. The deviation of S_{Hmax} with respect to S_{HRmax} is defined by the γ angle (Figure 7a).

[46] Lithospheric structure in the Gibraltar Arc shows severe changes in crustal and lithospheric thickness, important sedimentary depocenters and a large left-lateral strike-slip fault zone that runs through the arc crosscutting the orogenic trend. Next we discuss some of these features as possible sources of stress rotation in the Gibraltar Arc. The orientation of S_{Hmax} will depend on the relative magnitudes and azimuths of the regional (S_{HRmax}) and local (S_{HLmax}) stress components. As our data set includes diverse indicators that only provide information on stress orientation, we can only explore the nature of stress rotations qualitatively.

4.1.1. Crustal Thickness Variations

[47] Lateral changes in crustal thickness induce lateral density contrasts and therefore gradients in the gravitational potential energy field. Crustal thickness variations may promote tensional stresses parallel to the crustal thickening/thinning trend [e.g., *Zoback*, 1992] (Figure 7a). According to *Sonder*'s [1990] model, superposition of maximum horizontal stress caused by crustal thickness variations (S_{HLmax} parallel to Moho contours) on a regional stress field resulting from plate motion (S_{HRmax}, 134°) could locally deviate the regional stress trajectories resulting in S_{Hmax} rotations (γ angle) (Figure 7b). In this way, regions with N-S crustal thickening (i.e., E-W trending Moho contours) will produce an anticlockwise rotation of S_{Hmax} (Figure 7b). Conversely, E-W crustal thickness variations will induce a clockwise rotation.

[48] The deep structure of the Gibraltar Arc is characterized by a crustal bulge under the central Betics and sharp crustal thickness variations mostly coinciding with the North Alboran margin [*Torne and Banda*, 1992; *Banda et al.*, 1993; *Torne et al.*, 2000]. Although the lithosphere mantle structure could also be a source for stresses at shallow crustal levels [*Zoback and Mooney*, 2003], we have only explored the contribution of the crustal structure on the stress field. On the basis of the crust thickness model proposed by *Torne et al.* [2000] we computed the slope gradients of the Moho surface (Figure 8a). The steepest gradients of crustal thickness occur in a narrow and arched band centered on the coastlines, with maximum values (slope >30°) on the North Alboran margin and the Strait of Gibraltar.

[49] Considering >15° deviations as rotations, Figure 8b compares rotations (γ angle) observed in the region with expected rotations due to crustal thickness variations. This model has been calculated for those regions with the highest Moho slope (≥20°) as likely sources of stress perturbation. Stress orientations observed on the North Alboran margin match the model prediction and reinforce the interpretation that the crustal structure acts here as a likely source of stress rotation. On the contrary, this model does not fit with the data in domains like the Cartagena margin (1.5°−0.5°W, 37.5°N) and the Alhoceima region (4°W, 35°N) where a clockwise stress rotation is inferred and the observations show a gentle to moderate anticlockwise rotation of S_{Hmax} ($45° < \gamma > 15°$). On the North Alboran margin an isolated indicator in the offshore region (station number 25; Figure 6a), which indicates clockwise rotation ($\gamma = 42°$), is close to the southern limit of the region with predicted anticlockwise rotation. The discrepancy between the model prediction and the observations in these regions may suggest the participation of local preexisting structures. Thus further analysis with other stress sources should be done to unravel such stress rotations.

[50] It is significant that normal faulting stress indicators are confined to the high-elevation domains in the central Betics. This region coincides with maximum crustal thickness (Figure 8a), thus resulting in a maximum gravitational potential energy (GPE) domain. Excess of GPE induces perturbation of the stress field moving the σ_1 axis toward the vertical, promoting high-angle normal faulting processes [e.g., *Molnar and Lyon-Caen*, 1988; *Flesch et al.*, 2000, 2001]. It is thus demonstrated that topography and its compensation at depth by a crustal bulge condition the tectonic style of the central Betics.

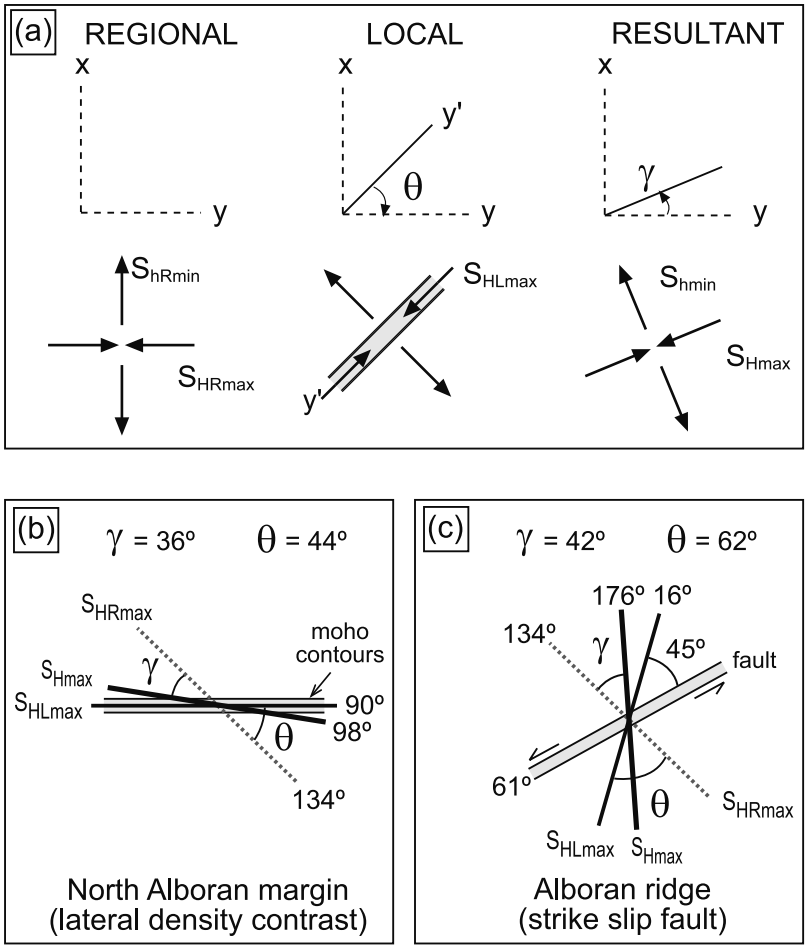

Figure 7. (a) Geometric relations used to estimate in the resulting maximum horizontal stress (S_{Hmax}) the interaction between a local source of stress (S_{HLmax}) and the regional stress (S_{HRmax}) (modified from *Zoback* [1992]). (b) Stress rotation due to the crustal structure. (c) Stress rotation within a strike-slip fault zone. The parameter γ is the angle between regional (S_{HRmax}) and maximum horizontal stresses (S_{Hmax}). The parameter θ is the angle between the regional stress field (S_{HRmax}) and the local stress (S_{HLmax}). The position of both examples is indicated with labeled boxes in Figure 8b. S_{HRmax} is taken from NUVEL-1A [*DeMets et al.*, 1994].

4.1.2. Sediment Loading

[51] Sediment loading is also a potential source of flexural stress affecting the regional stress field [e.g., *Walcott*, 1972; *Cloetingh et al.*, 1982; *Stein et al.*, 1989]. The thick sedimentary depocenter that constitutes the West Alboran Basin (>8 km) and its northeastern continuation along the Spanish shelf (Figure 8b) could also become a source of stress, with more significant effects in offshore regions. Rotation from the regional stress field would increase westward with sediment thickness [*Soto et al.*, 1996; *Torne et al.*, 2000]. Since major depocenters in the Alboran Sea mimic the crustal structure, both sediment loading and density contrasts buoyancy forces similarly influence the stress field along the North Alboran margin, making it difficult to estimate the amount of rotation due to each cause.

Figure 8. (a) Gradients of crustal thickness variation in the Gibraltar Arc and synthetic stress regime map based on Figure 6. Moho contour lines (in km) are taken from Figure 3. Stress indicators from isolated C quality stress data are not included. (b) Domains of predicted stress rotation due to the crustal structure for those areas with the steepest gradients of crustal thickening (slope >20°): clockwise rotations in blue and anticlockwise in red. The number inside the circles indicates the amount and sense of rotation observed and the color scale gives a semiquantitative assessment of rotations (Figure 6b). Major strike-slip fault segments active during the Quaternary throughout the Gibraltar Arc are highlighted (sources in the text): ALF, Alpujarras fault zone; AF, Alhoceima fault zone; AMF, Alhama de Murcia fault, ARF, Alboran Ridge fault, CF, Carboneras fault; JF, El-Jebha fault; MF, Maro-Nerja fault zone; NF, Nekor fault; PF, Palomares fault; YF, Yusuf fault. Large arrows correspond to the Africa-Eurasia relative motion according to NUVEL-1A [*DeMets et al.*, 1994]. Boxes labeled (b) and (c) correspond to Figure 7 sketches. AB, Algerian Basin; AR, Alboran Ridge; EAB, East Alboran Basin; SAB, South Alboran Basin; WAB, West Alboran Basin. Major sedimentary depocenters (in green) are taken from Figure 2.

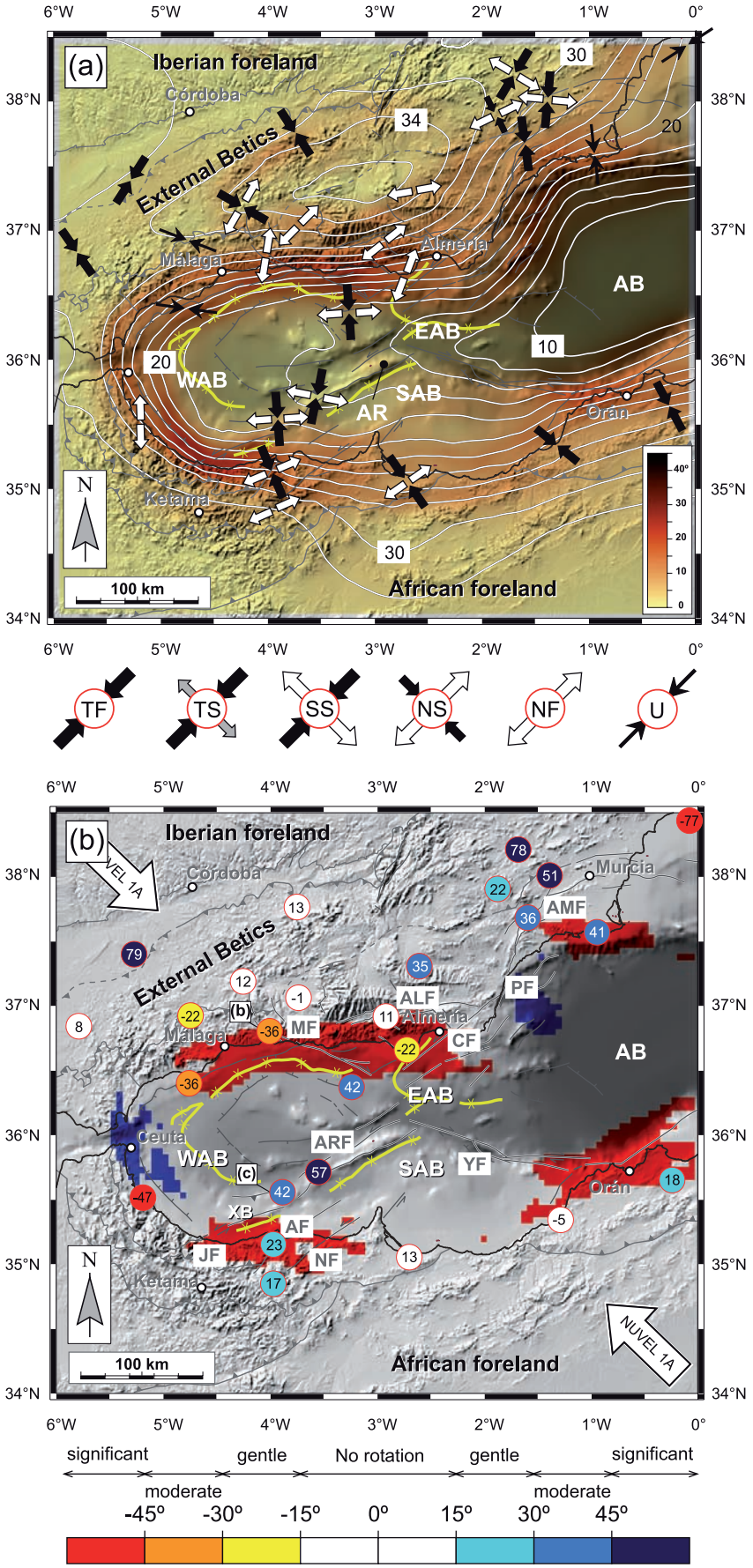
(a)
Iberian foreland
Córdoba
External Betics
Málaga
Almería
AB
EAB
WAB
SAB
AR
Orán
Ketama
African foreland
100 km
N
TF
TS
SS
NS
NF
U
(b)
Iberian foreland
VEL 1A
Murcia
AMF
ALF
PF
CF
MF
ARF
YF
XB
AF
JF
NF
Ceuta
NUVEL 1A
significant
gentle
No rotation
moderate
-45º
-30º
-15º
0º
15º
30º
45º

Figure 8

[52] The Guadalquivir Basin and Rharb Basin, which are the respective foreland basins of the Betic and Rif branches of the orogen, represent the most important sediment accumulation after the Alboran Sea Basin. Sedimentary thickness is over 3 km in the Guadalquivir Basin [*García-Castellanos et al.*, 2002] and ~2 km in the Rharb Basin [*Zizi*, 2002; *Zouhri et al.*, 2002]. Stress field patterns in both basins may be influenced by flexural stresses due to their sedimentary loads. Unfortunately, we have no stress indicators in the Rharb Basin and the few in the Guadalquivir area are quite scattered with low-quality data. It is therefore hard to characterize the role of sediment loading as a source of stress in these foreland basins.

4.1.3. Active Strike-Slip Faulting

[53] In the eastern Betics and parts of the Rif region (Figure 2) important left-lateral strike-slip faults were active throughout the Neogene [e.g., *Bousquet*, 1979; *Montenat et al.*, 1987; *Weijermars*, 1987; *de Larouzière et al.*, 1988; *Sanz de Galdeano*, 1990; *Sanz de Galdeano et al.*, 1995; *Masana et al.*, 2004]. These faults define a major strike-slip deformation zone (the Trans-Alboran Shear Zone, TASZ) whose nature, extent and character are under debate. The different segments of the TASZ run with a NE–SW trend from the eastern Betics (e.g., Alhama de Murcia, Palomares, and Carboneras faults) through the Alboran Sea along the bathymetric high of the Alboran Ridge and extend into the South Alboran margin with the El-Jebha and Alhoceima faults (Figure 8b). In detail these fault segments show complex interference and relay relationships, defining a long (~550 km) zone of strike-slip faulting oblique to the orogenic arc trend. In addition to this fault system, two major recent faults with NW–SE trend occur in the region. In the North Alboran margin, crosscutting the shoreline region, there is a major normal fault that continues NW with the Zafarraya fault. Both structures, although they do not connect according to surface geology, define a major, NW–SE trending deformation zone with normal and some left-lateral strike-slip motion (the Maro-Nerja fault zone; compare stations F-4 and F-6; Table 2). The Yusuf fault has similar orientation (WNW–ESE) and constitutes a narrow structure with recent (Quaternary) activity in the East Alboran Basin [*Alvarez-Marrón*, 1999]. This structure continues to the SE, connecting with the abrupt southern margin of the Algerian Basin, characterized by active, shallow reverse faulting [*Déverchère et al.*, 2005].

[54] The strength of large active strike-slip faults (especially plate-bounding transform faults) may influence the stress orientation resulting in a reorientation of the tectonic stress field close to the fault zone [*Zoback et al.*, 1987; *Zoback*, 1992; *Roy and Royden*, 2000; *Scholz*, 2000; *Miller*, 2002]. Similarly, the stress rotations we observed along the TASZ may represent a zone of weakness that localizes deformation. The reorientation of the stress field in their vicinity may suggest the low strength nature of the fault zone [e.g., *Townend and Zoback*, 2000]. The direction of maximum principal stress appears to rotate clockwise as the fault bends from NNE to NE trending in the eastern Betics ($\gamma = 36°$ to $51°$; Figure 8b). These observations agree with some previous studies using geological data to show the existence of clockwise rotations in the vicinity of these strike-slip faults [e.g., *Ott d'Estevou and Montenat*, 1985; *Martínez-Díaz*, 2002].

[55] In the Alboran Ridge strike-slip fault segment, there is evidence for moderate-to-significant clockwise stress rotations (e.g., $\gamma = 42°$ and $57°$ in Figure 8b) with respect to the regional stress field (Figure 8b). According to a model of stress orientation in the vicinity of weak (i.e., low frictional strength) strike-slip faults presented by *Ben-Avraham and Zoback* [1992], the direction of S_{Hmax} will rotate in the presence of the strike-slip fault, depending on the orientation of the far-field stress (S_{HRmax}) with respect to the fault and the strength of the fault in comparison to that of the surrounding crust. The regional angle (β) between the average strike of the Alboran Ridge fault zone (~60°) and the regional stress field (134°) is ~75°. In the context of the *Ben-Avraham and Zoback* [1992] model, variations of strike of the fault zone would result in changes from transpressive (local $\beta > 45°$) to transtensive deformations (local $\beta < 45°$). Transpressive deformation is in fact demonstrated to occur in most of the fault segments oriented NNE to NE (with $\beta > 45°$), such as along the Alhama de Murcia [*Martínez-Díaz*, 2002; *Masana et al.*, 2004], Palomares [e.g., *Booth-Rea et al.*, 2004], Carboneras [e.g., *Gràcia et al.*, 2006], Alboran Ridge [e.g., *Bourgois et al.*, 1992; *Watts et al.*, 1993] and Alhoceima faults. However, the Yusuf fault zone with its NW trend (i.e., $\beta < 45°$) proves to be a transtensive fault during the Quaternary [*Alvarez-Marrón*, 1999]. The stress rotations of S_{Hmax} we have reported in the vicinity of these fault segments therefore agree with the expected changes for a low-frictional strength left lateral fault zone within the regional field. Such low frictional strength of the faults in the Alhoceima region has also been suggested by recent INSAR analysis [*Akoglu et al.*, 2006]. The continuation of the TASZ to the south in this region requires a separate discussion because, according to the crustal model, it coincides with a domain with predicted anticlockwise rotation (Figure 8).

[56] The southwestern end of the Alboran Ridge fault segment is characterized by two major structures (Figure 8b): the WSW–ENE topographic high of the Xauen Bank, which continues onshore with the El Jebha fault, and the Alhoceima region, where high-angle, strike-slip to normal faults [*Medina*, 1995; *Aït-Brahim et al.*, 2002] are associated with shallow seismicity [*Calvert et al.*, 1997; *Bezzeghoud and Buforn*, 1999; *Hahou et al.*, 2004; *Stich et al.*, 2005]. In the Xauen Bank there is evidence for Pliocene to recent NNW–SSE compression associated with active folding and ENE-WSW high-angle strike-slip and reverse slip faults that deform both shallow sedimentary sequences and the seafloor [*Bourgois et al.*, 1992; *Watts et al.*, 1993; *Chalouan et al.*, 1997]. The age of the left-lateral El Jebha strike-slip fault is still debated [e.g., *García-Dueñas et al.*, 1992; *Platt et al.*, 2003]. Considering the crustal structure in the central and eastern Rif (5°–4°W), a local anticlockwise rotation of S_{Hmax} is expected with respect to the regional (S_{HRmax}) trend (Figure 8b). However, a gentle (17°–23°) clockwise rotation is observed in the Alhoceima region. It could therefore be suggested that crustal structure and active faulting along the TASZ counteract each other here, most probably with a more significant contribution from active strike-slip faulting.

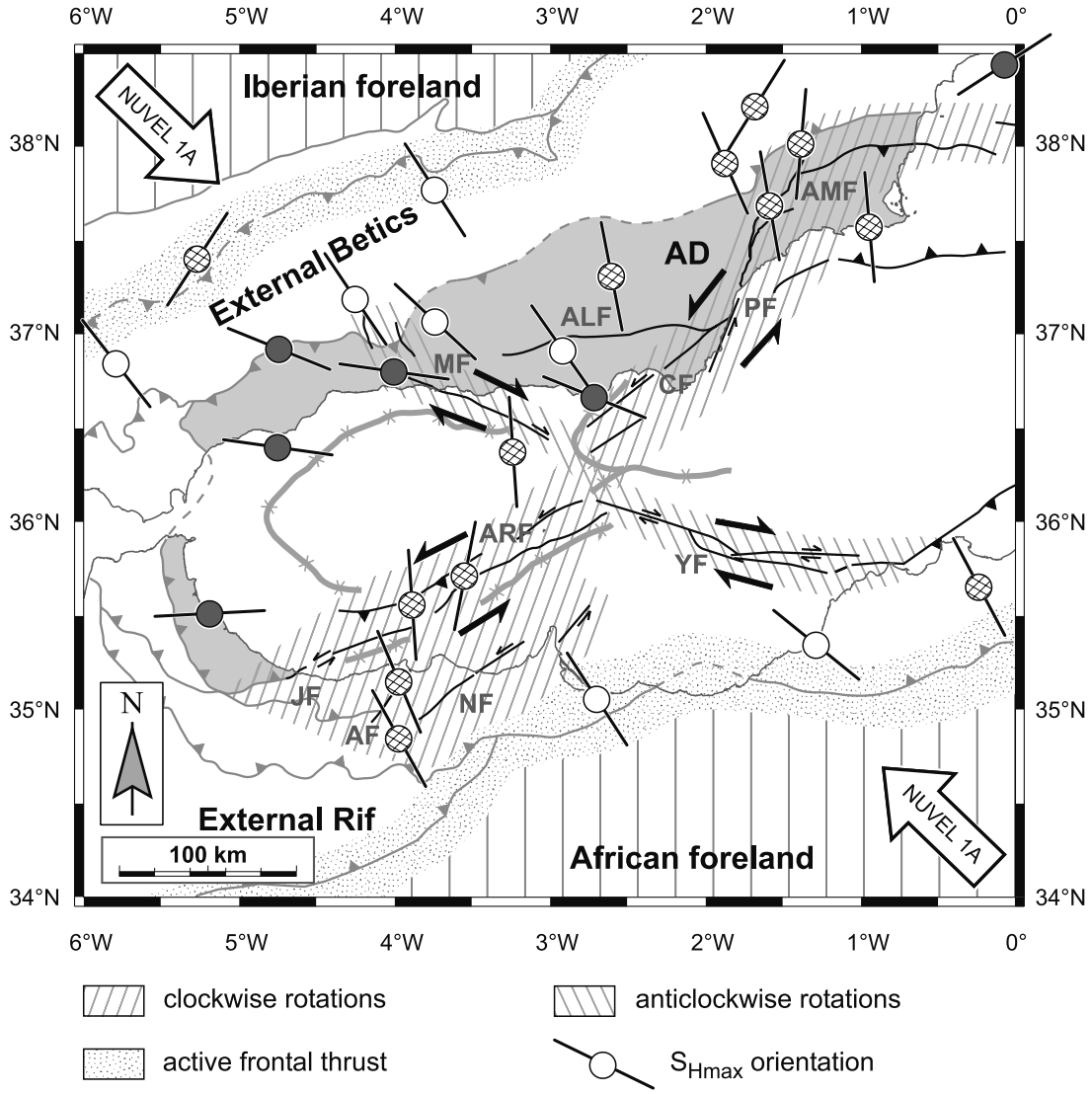

Figure 9. Tectonic sketch map of the Gibraltar Arc showing the active fault structure, the associated stress rotations, and suggested mode of deformation partitioning within the Africa-Eurasia plate boundary. S_{Hmax} orientation and stress rotation with respect to the regional stress field are taken from Figure 8 (net in circles, clockwise rotation; dark grey, anticlockwise rotation; white, no rotation). Geology is simplified from Figure 2. AD, Alboran Domain; ALF, Alpujarras fault zone; AF, Alhoceima fault zone; AMF, Alhama de Murcia fault; ARF, Alboran Ridge fault; CF, Carboneras fault; JF, El-Jebha fault; MF, Maro-Nerja fault zone; NF, Nekor fault; PF, Palomares fault; YF, Yusuf fault. Major sedimentary depocenters are taken from Figure 2.

4.2. Geodynamic Implications

[57] The data set and interpretations we present can be used to test some of the implications of the different geodynamic models on the recent tectonics of the Gibraltar Arc. We now discuss whether some indication can be provided on the mode of deformation partitioning in the arc, how the deforming regions and their stress field characteristics can be established and what the sources of stress perturbation are there.

[58] It is well established that the Neogene evolution of the western Mediterranean region is conditioned by the westward migration of the Gibraltar Arc [*Platt et al.*, 2003, and references therein]. This process promotes differential rotations of the northern and southern branches, predicting finite clockwise rotation in the Betics and anticlockwise in the Rif [*Royden*, 1993; *Lonergan and White*, 1997]. Recent paleomagnetic determinations in the arc confirm this [*Platt et al.*, 2003; *Mattei et al.*, 2006]. If thrusting remains active in the orogenic front, differential stress rotations should be observed.

[59] The general pattern of stress, the location of active structures and the distribution of the different stress sources in the Gibraltar Arc are summarized schematically in Figure 9. The stress orientations we present depict the situation in the frontal thrust of the External Betics (near the Guadalquivir Basin) and in the Tell region. In both cases, the overall stress orientation is congruent with Africa-Eurasia plate convergence (stress rotations show gentle or

no rotation values, Figure 8b), suggesting active deformation (mainly by thrusting) in the External front throughout the Gibraltar Arc. Available stress indicators south of the studied region in the front of the External Rif (e.g., at Saïss Basin [*Bargach et al.*, 2004]) corroborate the probably active nature of this thrust front. Local, but significant, stress rotations in portions of the external arc front suggest active deformation along preexisting structures like blind thrusts.

[60] Additionally, the existence of a major strike-slip fault zone with a NE trend is confirmed crosscutting the arc, from the eastern Betics to the Alhoceima region in the Rif (Figure 9). Throughout this wide zone of complex deformation, we show the existence of active transpressive (left-lateral) faulting and moderate-to-significant clockwise stress rotations ($\gamma > 30°$). This fault system (the Trans Alboran Shear Zone, TASZ) was already known to be active throughout the Neogene, contributing to the westward advance of the Gibraltar Arc [e.g., *Bousquet*, 1979; *Leblanc and Olivier*, 1984; *Sanz de Galdeano*, 1990; *Martínez-Díaz*, 2002; *Masana et al.*, 2004]. Our results demonstrate that some of the previous fault segments are currently active. The TASZ constitutes a key element to interpret the present-day tectonics of the western Mediterranean region. Oblique to the TASZ, two major fault systems with NW trend and right-lateral strike-slip faulting (the Maro-Nerja and the Yusuf faults; Figure 9) have associated transtensive deformation.

[61] The overall pattern of stress and the inferred motion of the two fault systems suggest the lateral escape in opposite directions of two domains. The Gibraltar Arc itself is thought to escape to the west (NW in the External Betics and S-SW in the External Rif), whereas the Tell, separated from the Rif by a major element of the African foreland, could move to the SSE-SE. This proposition agrees with recent GPS determination on the western front of the Gibraltar Arc and eastern Betics [*Fadil et al.*, 2006; *Stich et al.*, 2006], although it should be contrasted with detailed stress observations in other sectors such as the eastern Rif, the Tell and the Gulf of Cadiz regions.

5. Conclusions

[62] We constructed a general model of the present-day stress field in the Gibraltar Arc in the westernmost Mediterranean (Betic-Rif chains and Alboran Sea) based on information from different types of stress indicators (borehole breakouts, hydraulic fracturing, fault slip data and focal mechanism data). The present-day stress field reported in this paper does not match the fan-shaped pattern of S_{Hmax} typical of the stress field in other orogenic belts (indicating compression radial to the orogen) and is mostly constrained by the regional stress field imposed by the NW–SE Africa-Eurasia plate convergence.

[63] In some regions, deviations of S_{Hmax} are observed with respect to the regional stress field. These are gentle-to-moderate (22°–36°) anticlockwise rotations located along the North Alboran margin and moderate-to-significant (36°–78°) clockwise rotations along a major left-lateral fault zone that crosscut the entire Gibraltar Arc (the Trans-Alboran Shear Zone (TASZ)). The observed stress pattern is probably the consequence of the interference between different types of stress sources: (1) ongoing convergence between the African and Eurasian plates in the western Mediterranean; and (2) secondary stress sources arising from the crustal structure and/or important sedimentary accumulations and an active strike-slip fault zone.

[64] Sharp variations of crustal thickness across the Alboran Sea margins result in horizontal density contrasts between the crust and an anomalous lithosphere mantle and also in high gradients of the GPE stored in the lithospheric column. Maximum variations of crustal thickness are located along the northern Alboran Sea coastline and are a likely source of local stress causing moderate stress rotations in a narrow zone centered on the North Alboran margin. The thick sedimentary depocenter that constitutes the West Alboran Basin could also influence the stress field along this margin in the same way.

[65] The TASZ, running across the eastern Gibraltar Arc from the Betics to the Alhoceima region in the Rif, consists of NE-SW segments with a relay pattern shaping a long, complex zone of strike-slip faulting (~550 km) with left-lateral motion. If it has low strength, it would induce a clockwise rotation of the regional stress field. Local stress rotations in the Alboran Sea Basin, where there is a flat Moho, provide a clue to confirm that this major strike-slip system may have low frictional strength and constitute a major active structure in the complex Africa-Eurasia plate boundary zone. The TASZ and the Maro-Nerja and Yusuf systems condition lateral escape of the Gibraltar Arc to the west within a regional plate convergence setting, thus representing key elements for understanding of present-day deformation partitioning in the western Mediterranean.

Appendix A: Borehole Breakout Analysis

[66] Four arm caliper data were processed with GMI·CALIPER^{TM} software that allowed us to obtain the mean direction with a standard deviation value of the breakout distribution throughout the well. The software also provided a rose diagram, a histogram, and a well section plot with the breakouts projection (Figure A1).

[67] At a first stage, we inspected the caliper arms orientation along the entire well, discarding those intervals where the arms were trapped in key seats. We also considered well deviation to avoid hole enlargements in wells deviating more than 4°, thus coinciding with the high side of the borehole.

[68] Once these intervals had been discarded, we compared the logging data with depth distribution of breakouts. For each analyzed well we considered the depth and the lithology in which the breakouts were detected, as well as the logging data available. As a general analytical procedure, we selected logging data (when available) from gamma ray, bulk density, resistivity and sonic logs. These data together with the lithological description of the well are quite useful to validate the breakout results. Usually we detected stress rotations along the well by comparing breakout rotation intervals with the logging data, trying to identify the source of these rotations. Rotations may be related to the presence of fault zones, which are well imaged by logging data (e.g., low seismic velocities, density decreases, high gamma ray values, low resistivity) or have a lithological control.

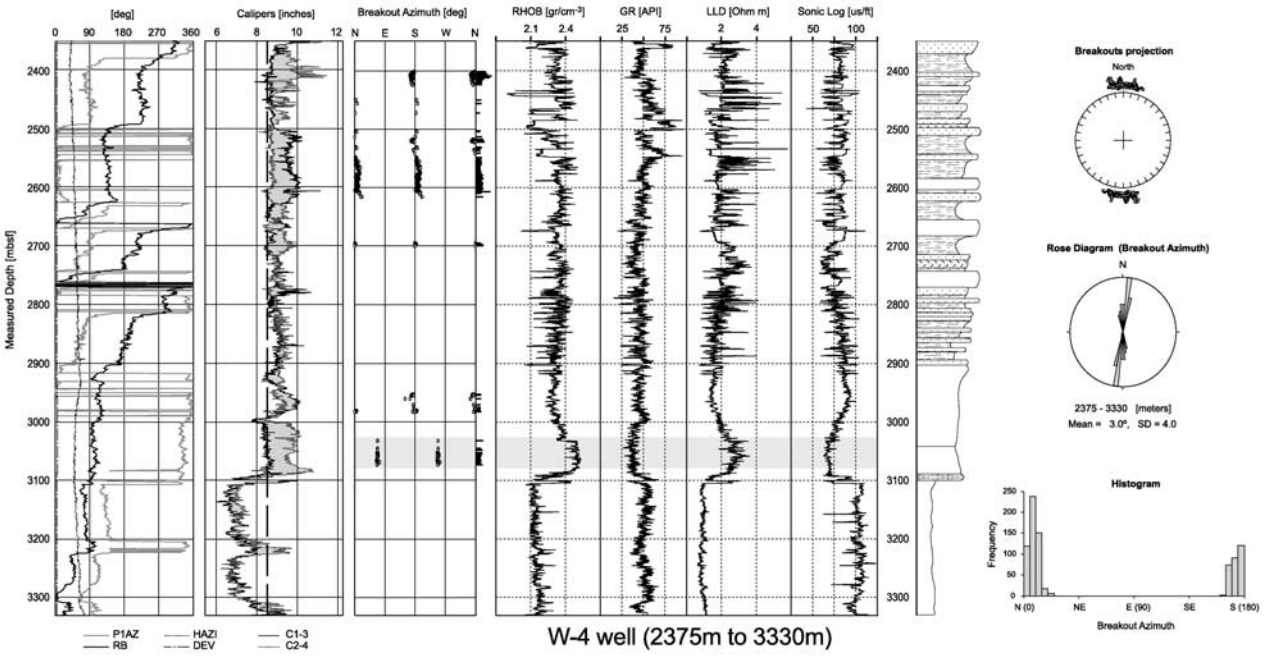

Figure A1. Four-arm caliper data from HDT tool at the 2375–3330 m interval of the W-4 well: DEV (hole deviation), HAZI (hole azimuth), RB (regular bedding), P1AZ (pad 1 azimuth), C1-3 (caliper 1), and C2-4 (caliper 2). Breakout azimuth inferred for this section is compared with other logging data and with the lithological column. Breakout rotation between 3000 m (meters below seafloor) and 3100 m agree with well-defined variations in the logging record. Main results of computed circular statistics as well as breakout projection around the hole are shown at the right-hand side.

[69] As an example of the general analysis procedure we applied in each well to calculate the mean S_{Hmax} orientation, Figure A1 illustrates the case of well W-4 (see location in Figure 2). The stratigraphic column for this section (2375 m to 3330 m) is mainly composed of clays and fine grain sands with a few volcano-sedimentary layers (2375–2550 m), sand and conglomerates with interbedded clays (2550–2920), calcareous clays and minor siltstones increasing toward the bottom of the formation (2920–3100 m) and clays and minor interbedded siltstones (3100–3330 m).

[70] This well exhibits a 50 m thick interval where breakouts show a sudden rotation (3025–3075 m interval). In order to evaluate the possible source of breakout rotations in this interval, we compared the logging data, the lithological descriptions and the breakout orientations. Breakout rotations in this interval may be related to a key seat zone produced by some lithological changes according to the logging record. Note that the small caliper is slightly below bit size and P1AZ is fixed; thus C1-3 is trapped in a key seat. Therefore we have not considered this interval to compute the mean breakout orientation within the hole.

[71] Mean breakout azimuth along the W-4 well (2375–3330 m interval) is 003° ± 04°, thus resulting in a N93°E orientation of S_{Hmax}. Since this well was drilled in 1983, we applied the appropriate magnetic declination correction to the inferred S_{Hmax} azimuth (Table 1).

Appendix B: Focal Mechanism Data

[72] A set of 81 focal mechanisms from crustal earthquakes was compiled for this study (Figure B1). Most of the data come from the Instituto Andaluz de Geofísica (IAG) database (http://www.ugr.es/~iag). All these focal mechanisms were considered reliable since they were calculated through moment tensor inversion (see method and detailed explanation by *Stich et al.* [2003]). Focal mechanism information is found throughout the entire region, as is seismicity (Figure 3), and describes the following pattern along the Gibraltar Arc. The South Alboran margin and the Algerian margin are characterized by the occurrence of most of the high-magnitude events of the western Mediterranean in recent years, e.g., 2004 Alhoceima (Morocco, M_w = 6.3), 1994 Mascara (Algeria, M_w = 5.7), and 1992 Melilla (Spain, M_w = 4.8) [e.g., *Bezzeghoud and Buforn*, 1999]. Algerian earthquakes show focal mechanisms with a clear predominance of the reverse slip type. Along the South Alboran margin data tend to concentrate in the Alhoceima region, where tensor solutions mainly correspond to strike-slip faults with few normal faults southward (Figure B1). In the Alboran Sea seismicity nucleates along the Alboran Ridge and the East Alboran Basin. Focal mechanisms here mostly correspond to strike-slip faults, but often P, B and T axes display moderate plunges so it is difficult to specify the regime (U category in Table B1). In the Betics the seismic pattern becomes complex and the tectonic regimen varies from normal to thrust faulting along the orogen (Figure B1). In the eastern Betics strike-slip faulting predominates, with a minor normal or thrust component. Eventually thrust faulting occurs due to bending of the strike-slip fault system running across this region. In the central Betics, around the high mountain ranges, the P axes

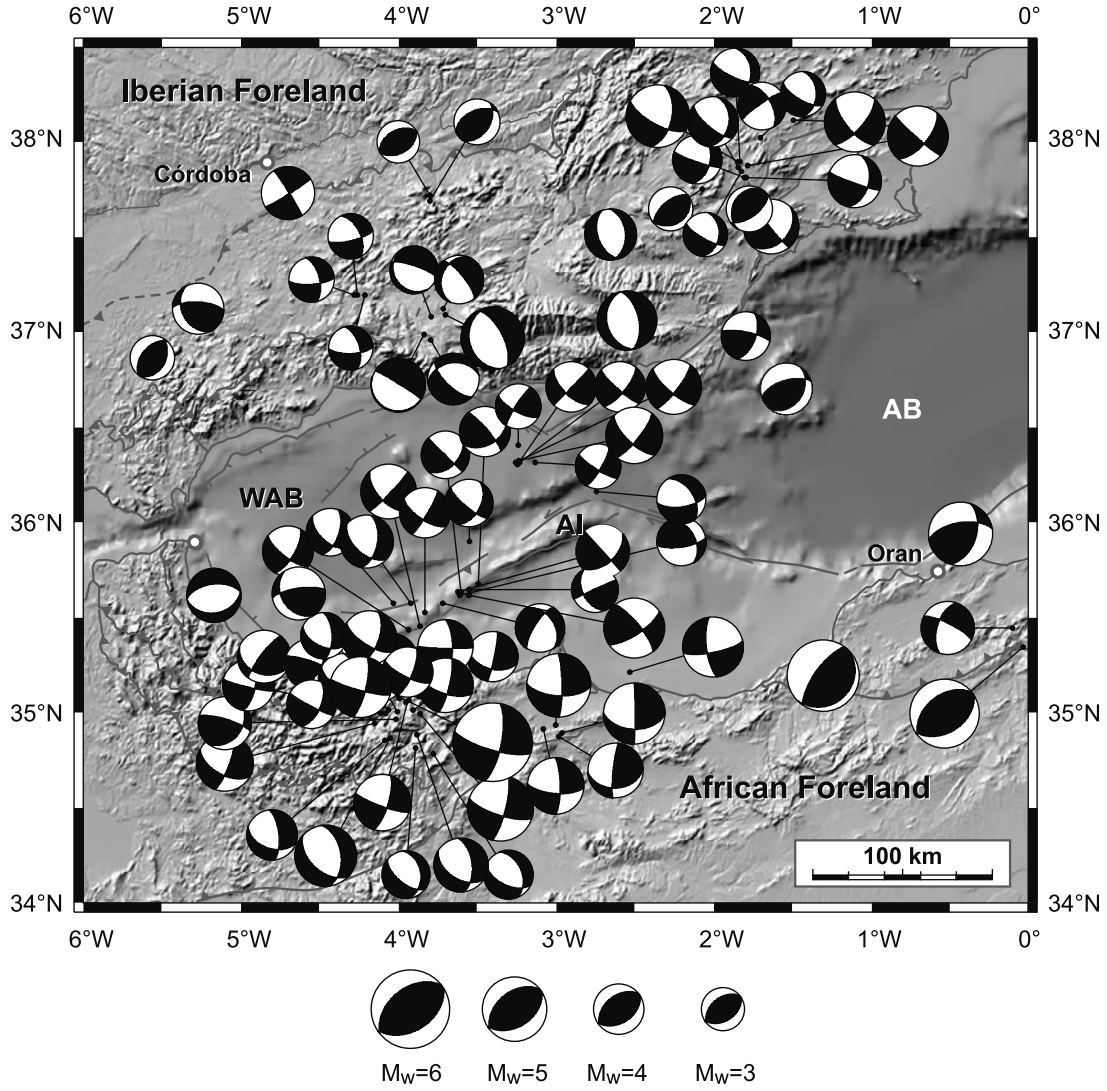

Figure B1. Crustal focal mechanisms from moment tensor inversion for 81 events in lower hemisphere equal-area projection compiled for the Gibraltar Arc in the last 20 years. Dilatational quadrants are plotted in white. Earthquake details are summarized in Table B1. AB, Algerian Basin; AI, Alboran Island; WAB, West Alboran Basin.

Table B1. Focal Mechanism Data Compiled for This Study[a]

Num.	Date	Longitude	Latitude	P Axis	B Axis	T Axis	Regime	Z (km)	M_w	Station[b]
1	27/05/2000	−3.13	36.36	18/347	72/168	00/077	SS	16	3.6	FM-1
2	07/08/1997	−3.24	36.45	08/344	69/233	20/077	SS	16	3.6	FM-1
3	03/07/1997	−3.23	36.36	20/257	69/185	06/265	SS	10	4.0	FM-1
4	02/07/1997	−3.24	36.35	21/356	63/220	17/093	SS	8	4.0	FM-1
5	02/07/1997	−3.26	36.36	21/354	69/185	04/085	SS	10	4.4	FM-1
6	02/07/1997	−3.24	36.37	26/354	63/188	06/087	SS	6	4.5	FM-1
7	02/03/2004	−3.87	35.14	26/328	62/171	09/063	SS	12	4.4	FM-2
8	27/02/2004	−3.99	35.13	20/324	68/164	07/056	SS	14	4.4	FM-2
9	27/02/2004	−3.96	35.13	16/328	72/122	07/235	SS	12	4.3	FM-2
10	27/02/2004	−3.92	35.18	19/334	71/141	04/242	SS	14	4.5	FM-2
11	25/02/2004	−3.94	35.17	24/339	66/159	00/249	SS	10	4.0	FM-2
12	24/02/2004	−3.91	35.07	32/321	49/186	24/066	SS	10	4.0	FM-2
13	24/02/2004	−3.95	35.11	21/320	69/142	01/050	SS	16	4.0	FM-2
14	24/02/2004	−4.08	35.17	38/343	51/156	04/250	SS	16	4.3	FM-3
15	18/07/1999	−4.10	35.24	26/346	58/129	16/247	SS	10	3.9	FM-3
16	26/02/2004	−4.06	35.19	17/330	72/138	03/239	SS	16	4.9	FM-3
17	10/07/2004	−4.07	35.16	53/320	37/154	07/059	NF	6	3.7	FM-3
18	20/10/1998	−3.78	34.84	67/328	22/133	05/225	NF	6	3.9	FM-4
19	14/08/2004	−3.89	34.87	65/353	22/142	12/237	NF	6	3.8	FM-4
20	20/06/2004	−3.88	34.94	61/231	29/153	05/060	NF	4	3.9	FM-4

Table B1. (continued)

Num.	Date	Longitude	Latitude	P Axis	B Axis	T Axis	Regime	Z (km)	M_w	Station[b]
21	10/10/2004	−4.06	35.07	03/329	79/075	11/239	SS	22	4.0	FM-5
22	06/04/2004	−4.11	35.05	28/331	31/223	46/094	U	6	4.2	FM-5
23	01/04/2004	−4.10	35.09	17/343	51/095	34/242	SS	8	4.0	FM-5
24	07/03/2004	−4.01	35.06	13/318	77/137	00/228	SS	22	5.0	FM-5
25	24/02/2004	−4.08	35.05	21/330	66/122	10/236	SS	10	4.1	FM-5
26	22/02/2003	−3.55	35.70	28/010	46/247	31/118	SS	4	3.7	FM-6
27	21/02/2003	−3.62	35.69	27/010	51/138	26/266	SS	4	4.2	FM-6
28	21/02/2003	−3.60	35.69	30/008	46/136	28/260	SS	2	3.8	FM-6
29	19/02/2003	−3.49	35.73	22/018	43/080	39/269	SS	4	4.0	FM-6
30	18/02/2003	−3.61	35.67	17/200	39/096	47/308	TS	2	3.9	FM-6
31	28/11/2000	−3.72	35.63	50/163	34/019	18/276	NS	6	3.9	FM-6
32	18/11/1998	−3.79	36.99	60/083	24/302	17/204	NF	8	4.1	FM-7
33	10/09/2003	−3.79	37.11	58/186	09/291	30/026	NF	12	3.8	FM-7
34	24/02/1997	−3.83	37.02	49/212	00/122	41/032	U	19	4.3	FM-7
35	28/12/1996	−3.71	37.15	55/202	24/330	24/072	NF	12	3.9	FM-7
36	24/06/1984	−3.70	37.12	71/231	5/336	18/068	NF	6	5.0	FM-7
37	14/04/1998	−4.21	37.22	40/310	50/116	07/214	SS	12	3.5	FM-8
38	13/04/1998	−4.26	37.22	37/301	50/098	12/202	SS	14	3.6	FM-8
39	13/04/1998	−4.28	37.22	34/309	55/115	07/215	SS	14	3.6	FM-8
40	24/06/2002	−3.79	37.73	02/321	16/051	74/223	TF	2	3.7	FM-9
41	24/06/2002	−3.77	37.73	00/330	00/060	90/270	TF	2.5	3.4	FM-9
42	06/08/2002	−1.83	37.90	57/346	27/127	18/227	NF	6	3.9	FM-10
43	07/08/2002	−1.84	37.87	48/359	31/132	25/238	U	6	4.0	FM-10
44	07/08/2002	−1.82	37.85	50/009	18/123	34/225	NS	6	3.5	FM-10
45	03/02/2005	−1.79	37.82	34/342	45/116	25/234	U	10	4.2	FM-10
46	04/02/2005	−1.80	37.82	35/340	46/117	23/232	SS	6	3.9	FM-10
47	22/03/2005	−2.98	34.93	29/305	36/191	40/063	U	6	4.4	FM-11
48	09/12/2004	−3.08	34.97	26/314	63/153	08/048	SS	12	4.5	FM-11
49	04/12/2004	−3.00	34.99	26/313	60/165	14/050	SS	12	5.1	FM-11
50	02/12/2004	−2.96	34.95	30/307	47/178	27/055	U	8	4.9	FM-11
51	15/02/2003	−3.83	35.58	23/345	65/192	10/172	SS	12	4.0	FM-12
52	06/07/2002	−3.92	35.63	56/338	34/164	03/073	NF	18	4.2	FM-12
53	27/06/2002	−4.03	35.63	48/343	41/170	03/077	NS	14	3.8	FM-12
54	08/06/2001	−3.93	35.49	26/349	60/166	02/259	SS	8	4.0	FM-12
55	05/10/1988	−3.86	35.51	26/355	58/213	17/094	SS	8	4.4	FM-12
56	18/02/2003	−3.55	35.67	03/009	67/106	12/077	SS	4	4.8	FM-13
57	13/08/2000	−3.55	35.95	40/357	46/145	16/253	SS	14	3.8	FM-14
58	29/05/1999	−2.74	36.21	51/303	38/106	08/202	NS	6	3.9	FM-15
59	27/02/2004	−3.92	35.18	19/334	71/131	04/242	SS	14	4.5	FM-16
60	25/02/2004	−3.86	35.05	21/330	69/159	03/061	SS	10	5.2	FM-17
61	20/03/2004	−4.15	35.00	34/334	53/182	14/073	SS	10	4.5	FM-18
62	12/03/2004	−4.05	34.92	70/331	20/154	01/063	NF	6	4.9	FM-19
63	24/02/2004	−4.00	35.14	25/329	65/148	01/239	SS	14	6.3	FM-20
64	04/02/2002	−2.55	37.09	78/262	01/167	12/077	NF	10	4.7	FM-21
65	06/04/1998	−1.79	37.01	11/335	55/081	33/237	SS	8	3.9	FM-22
66	16/11/2003	−2.65	37.53	81/015	08/168	04/259	NF	8	4.1	FM-23
67	25/07/2003	−5.56	36.90	06/305	05/035	83/165	TF	6	3.5	FM-24
68	24/01/2003	−4.70	37.74	06/283	84/104	00/013	SS	12	4.2	FM-25
69	30/06/2005	−1.57	36.68	15/327	18/062	66/201	TF	3	3.8	FM-26
70	06/08/2002	−1.84	37.90	43/325	46/158	07/061	NS	8	5	FM-27
71	29/01/2005	−1.78	37.88	23/359	62/142	15/263	SS	10	4.8	FM-28
72	18/08/1994	−0.03	35.40	00/324	04/234	86/058	TF	4	5.7	FM-29
73	12/03/1992	−2.53	35.27	23/131	67/303	03/040	SS	30	4.8	FM-30
74	02/02/1999	−1.49	38.11	33/360	57/185	02/092	SS	6	4.8	FM-31
75	14/08/1999	−1.69	38.18	30/187	55/041	16/287	SS	6	3.8	FM-32
76	02/08/2000	−1.77	37.66	16/135	10/228	71/349	TF	4	3.7	FM-33
77	13/07/1967	−0.43	35.89	11/329	26/064	61/217	TF	5	5.1	FM-34
78	19/04/1981	−0.10	35.50	33/162	54/316	13/064	SS	16	4.2	FM-35
79	15/09/2002	−5.27	37.16	17/026	29/285	05/142	TF	4	4.1	FM-36
80	22/12/1999	−1.28	35.32	26/307	10/213	62/103	TF	8	5.7	FM-37
81	04/08/1999	−5.17	35.57	80/179	01/083	10/353	NF	10	4.3	FM-38

[a]These data are plotted in Figure B1. NF, normal faulting; NS, predominantly normal faulting with strike-slip component; SS, strike-slip faulting; TS, predominantly thrust faulting with strike-slip component; TS, thrust faulting.
[b]Stations are labeled in Figures 2 and 4.

rotate to a near vertical position resulting in a large area of normal faulting. To the west, in the Guadalquivir Basin and on its boundary with the External Betics, the tectonic regime is characterized by thrust faulting with a minor strike-slip component.

[73] **Acknowledgments.** This research is supported by the REN2001-3868-CO3MAR, CTM2005-08071-C03-01/MAR, and CSD2006-00041 projects and the Spanish program of Formación del Profesorado Universitario (Ministerio de Educación y Ciencia). We also want to thank the Stress and Crustal Mechanics Group (Stanford University) for providing additional support to this investigation. The authors wish to thank GeoMe-

chanics International (GMI) and A. Day-Lewis for helping with GMI·CALIPER™ software and J. D. López Valero (In Situ Testing S.L.) for providing the hydraulic fracturing data used in this paper. The manuscript benefited from the constructive comments of G. Rosenbaum, J. J. Martínez-Díaz, and an anonymous reviewer who are gratefully acknowledged. English grammar has been revised and improved by Ian MacCandless.

References

Aït-Brahim, L., et al. (2002), Paleostress evolution in the Moroccan African margin from Triassic to Present, *Tectonophysics*, *357*, 187–205.

Akoglu, A. M., Z. Cakir, M. Meghraoui, S. Belabbes, S. O. El Alami, S. Ergintav, and H. S. Akyüz (2006), The 1994–2004 Al Hoceima (Morocco) earthquake sequence: Conjugate fault ruptures deduced from InSAR, *Earth Planet. Sci. Lett.*, *252*, 467–480.

Alfaro, P., J. Galindo-Zaldívar, A. Jabaloy, A. C. López-Garrido, and C. Sanz de Galdeano (2001), Evidence for the activity and paleoseismicity of the Padul fault (Betic Cordillera, southern Spain), *Acta Geol. Hisp.*, *36*, 283–295.

Altamimi, Z., P. Sillard, and C. Boucher (2002), ITRF2000: A new release of the International Terrestrial Reference Frame for earth science applications, *J. Geophys. Res.*, *107*(B10), 2214, doi:10.1029/2001JB000561.

Alvarez-Marrón, J. (1999), Pliocene to Holocene structure of the eastern Alboran Sea (western Mediterranean), *Proc. Ocean Drill. Program Sci. Results*, *161*, 345–355.

Andreux, J., J. M. Fonboté, and M. Mattauer (1971), Sur un modele explicatif de l'Arc de Gibraltar, *Earth Planet. Sci. Lett.*, *12*, 191–198.

Angelier, J. (1979), Determination of the mean principal directions of stresses for a given fault population, *Tectonophysics*, *56*, T17–T26.

Angelier, J., and J. Goguel (1979), Sur une méthode simple de détermination des axes principaux des contraintes pour une population de failles, *C. R. Acad. Sci.*, *288*, 307–310.

Angelier, J., and P. Mechler (1977), Sur une méthode graphique de recherche des contraintes principales également utilisable en tectonique et en séismologie: La méthode des dièdres droits, *Bull. Soc. Geol. Fr.*, *7*, 1309–1318.

Armijo, R., E. Carey, and A. Cisternas (1982), The inverse problem in microtectonics and separation of tectonic phase, *Tectonophysics*, *82*, 145–160.

Azañón, J. M., and A. Crespo-Blanc (2000), Exhumation during a continental collision inferred from the tectonometamorphic evolution of the Alpujarride Complex in the central Betics (Alboran Domain, SE Spain), *Tectonics*, *19*, 549–565.

Bada, G., S. Cloetingh, P. Gerner, and F. Horvath (1998), Sources of recent tectonic stress in the Pannonian region: Inferences from finite element modeling, *Geophys. J. Int.*, *134*, 87–101.

Banda, E., J. Gallart, V. García-Dueñas, J. J. Dañobeitia, and J. Makris (1993), Lateral variation of the crust in the Iberian peninsula: New evidence from the Betic Cordillera, *Tectonophysics*, *221*, 53–66.

Bargach, K., P. Ruano, A. Chabli, J. Galindo-Zaldívar, A. Chalouan, A. Jabaloy, M. Akil, M. Ahmamou, C. Sanz de Galdeano, and M. Benmakhlouf (2004), Recent tectonic deformations and stresses in the frontal part of the Rif Cordillera and the Saïss basin (Fes and Rabat regions, Morocco), *Pure Appl. Geophys.*, *161*, 521–540.

Barton, C. A., and M. D. Zoback (1994), Stress perturbations associated with active faults penetrated by boreholes: Possible evidence for near-complete stress drop and a new technique for stress magnitude measurements, *J. Geophys. Res.*, *99*, 9373–9390.

Bell, J. S. (1990), Investigating stress regimes in sedimentary basins using information from oil industry wireline logs and drilling records, in *Geological Applications of Wireline Logs*, edited by A. Hurst, M. A. Lovell, and A. C. Morton. *Geol. Soc. Spec. Publ.*, *48*, 305–325.

Bell, J. S., and D. I. Gough (1979), Northeast-southwest compressive stress in Alberta—Evidence from oil wells, *Earth Planet. Sci. Lett.*, *45*, 475–482.

Bell, J. W., F. Amelung, and G. C. P. King (1997), Preliminary Late Quaternary slip history of the Carboneras fault, southeastern Spain, *J. Geodyn.*, *24*, 51–66.

Ben-Avraham, Z., and M. D. Zoback (1992), Transform-normal extension and asymmetric basins: An alternative to pull-apart models, *Geology*, *20*, 423–426.

Bezzeghoud, M., and E. Buforn (1999), Source parameters of the 1992 Melilla (Spain, M_w = 4.8), 1994 Alhoceima (Morocco, M_w = 5.8) and 1994 (Algeria, M_w = 5.7) earthquakes and seismotectonic implications, *B. Seismol. Soc. Am.*, *70*, 149–170.

Blanco, M. J., and W. Spakman (1993), The *P*-wave velocity structure of the mantle below the Iberian Peninsula: Evidence for a subducted lithosphere beneath southern Spain, *Tectonophysics*, *221*, 13–34.

Booth-Rea, G., J.-M. Azañón, A. Azor, and V. García-Dueñas (2004), Influence of strike-slip fault segmentation on drainage evolution and topography: A case study: The Palomares fault zone (southeastern Betics, Spain), *J. Struct. Geol.*, *26*, 1615–1632.

Bourgois, J. A., A. Mauffret, N. A. Ammar, and N. A. Demnati (1992), Multichannel seismic data imaging of inversion tectonics of the Alboran Ridge (western Mediterranean Sea), *Geo Mar. Lett.*, *12*, 117–122.

Bousquet, J. C. (1979), Quaternary strike-slip faults in southeastern Spain, *Tectonophysics*, *52*, 277–286.

Buforn, E., C. Sanz de Galdeano, and A. Udías (1995), Sismotectonics of the Ibero-Maghrebian region, *Tectonophysics*, *248*, 247–261.

Buforn, E., M. Bezzeghoud, A. Udías, and C. Pro (2004), Seismic Sources on the Iberia-African plate boundary and their tectonic implications, *Pure Appl. Geophys.*, *161*, 623–646.

Calvert, A., F. Gómez, D. Seber, M. Barazangi, N. Jabour, A. Ibenbrahim, and A. Demnati (1997), An integrated geophysical investigation of recent seismicity in the Al-Hoceima region of north Morocco, *Bull. Seismol. Soc. Am.*, *87*, 637–651.

Calvert, A., E. Sandvol, D. Seber, M. Barazangi, S. Roecker, T. Mourabit, F. Vidal, G. Alguacil, and N. Jabour (2000), Geodynamic evolution of the lithosphere and upper mantle beneath the Alboran Region of the western Mediterranean: Constraints from travel time tomography, *J. Geophys. Res.*, *105*, 10,871–10,898.

Campos, J., A. Maldonado, and A. C. Campillo (1992), Post-Messinian evolution patterns of the central Alboran Sea, *Geo Mar. Lett.*, *12*, 173–178.

Chalouan, A., R. Saji, A. Michard, and A. W. Bally (1997), Neogene tectonic evolution of the southwestern Alboran Basin as inferred from seismic data off Morocco, *AAPG Bull.*, *81*, 1161–1184.

Cloetingh, S., M. J. R. Wortel, and N. J. Vlaar (1982), Evolution of passive continental margins and initiation of subduction zones, *Nature*, *297*, 139–142.

Cloetingh, S., P. A. van der Beek, D. van de Rees, T. B. Roep, C. Biermann, and R. A. Stephenson (1992), Flexural interaction and the dynamics of Neogene extensional basin formation in the Alboran-Betic region, *Geo Mar. Lett.*, *12*, 66–75.

Coblentz, D., and R. M. Richardson (1996), Analysis of the South American intraplate stress field, *J. Geophys. Res.*, *101*, 8643–8657.

Coca, P., and E. Buforn (1994), Mecanismos focales en el Sur de España: Periodo 1965–1985, *Estad. Geol.*, *50*, 33–45.

Cocard, M., H. G. Kahle, Y. Peter, A. Geiger, G. Veis, S. Felekis, D. Paradissis, and H. Billiris (1999), New constraints on the rapid crustal motion of the Aegean region: Recent results inferred from GPS measurements (1993–1998) across the West Hellenic Arc, Greece, *Earth Planet. Sci. Lett.*, *172*, 39–47.

Comas, M. C., V. García-Dueñas, and M. J. Jurado (1992), Neogene extensional tectonic evolution of the Alboran Basin from MSC data, *Geo Mar. Lett.*, *12*, 157–164.

Comas, M. C., J. J. Dañobeitia, J. Alvarez-Marrón, and J. I. Soto (1995), Crustal reflections and structure in the Alborán Basin: Preliminary of the ESCI-Alborán Survey, *Rev. Soc. Geol. Esp.*, *8*(4), 529–542.

Comas, M. C., J. P. Platt, J. I. Soto, and A. B. Watts (1999), The origin and tectonic history of the Alboran Basin: Insights from Leg 161 results, *Proc. Ocean Drill. Program Sci. Results*, *161*, 555–580.

Cox, J. W. (1982), Long-axis orientation in elongated boreholes, *Tech. Rev.*, *30*, 15–25.

de Larouzière, F. D., J. Bolze, P. Bordet, J. Hernandez, C. Montenat, and P. Ott d'Estevou (1988), The Betic segment of the lithospheric trans-Alboran shear zone during the late Miocene, *Tectonophysics*, *152*, 41–52.

de Larouzière, F. D., P. A. Pezard, M. C. Comas, B. Celerier, and C. Vergniault (1999), Structure and tectonic stresses in metamorphic basement, Site 976, Alboran Sea., *Proc. Ocean Drill. Program Sci. Results*, *161*, 320–329.

Delacou, B., C. Sue, J.-D. Champagnac, and M. Burkhard (2004), Present-day geodynamics in the bend of the western and central Alps as constrained by earthquake analysis, *Geophys. J. Int.*, *158*, 753–774.

DeMets, C., R. G. Gordon, D. F. Argus, and S. Stein (1990), Current plate motions, *Geophys. J. Int.*, *101*, 425–478.

DeMets, C., R. G. Gordon, D. F. Argus, and S. Stein (1994), Effect of recent revisions to the geomagnetic reversal time scale on estimate of current plate motions, *Geophys. Res. Lett.*, *21*, 2191–2194.

Déverchère, J., et al. (2005), Active thrust faulting offshore Boumerdes, Algeria, and its relations to the 2003 M_w 6.9 earthquake, *Geophys. Res. Lett.*, *32*, L04311, doi:10.1029/2004GL021646.

Dewey, J. F. (1988), Extensional collapse of orogens, *Tectonics*, *7*, 1123–1139.

Dewey, J. F., M. L. Helman, E. Turco, D. H. W. Hutton, and S. D. Knott (1989), Kinematics of the western Mediterranean, in *Alpine Tectonics*, edited by M. P. Coward, D. Dietrich, and R. G. Park, *Geol. Soc. Spec. Publ.*, *45*, 265–283.

Duggen, S., K. Hoernle, P. van den Bogaard, L. Ruepke, and J. Phipps-Morgan (2003), Deep roots of the Messinian salinity crisis, *Nature*, *422*, 602–606.

Duggen, S., K. Hoernle, P. van den Bogaard, and C. Harris (2004), Magmatic evolution of the Alboran region: The role of subduction in forming the western Mediterranean and causing the Messinian Salinity Crisis, *Earth Planet. Sci. Lett.*, *218*, 91–108.

England, P. C., and G. Houseman (1986), Finite strain calculation of continental deformation: 1. Comparison with the India-Asia collision zone, *J. Geophys. Res.*, *91*, 3661–3663.

England, P. C., and P. Molnar (2005), Late Quaternary to decadal velocity fields in Asia, *J. Geophys. Res.*, *110*, B12401, doi:10.1029/2004JB003541.

Evans, K. (1989), Appalachian stress study: 3. Regional scale stress variations and their relation to structure and contemporary tectonics, *J. Geophys. Res.*, *94*, 17,619–17,645.

Faccenna, C., C. Piromallo, A. Crespo-Blanc, L. Jolivet, and F. Rossetti (2004), Lateral slab deformation and the origin of the western Mediterranean arcs, *Tectonics*, *23*, TC1012, doi:10.1029/2002TC001488.

Fadil, A., P. Vernant, S. McClusky, R. Reilinger, F. Gomez, D. Ben Sari, T. Mourabit, K. Feigl, and M. Barazangi (2006), Active tectonics of the western Mediterranean: Geodetic evidence for rollback of a delaminated subcontinental lithosphere slab beneath the Rif Mountains, Morocco, *Geology*, *34*, 529–532.

Faulkner, D. R., A. C. Lewis, and E. H. Rutter (2003), On the internal structure and mechanics of large strike-slip fault zones: Field observations of the Carboneras fault in southeastern Spain, *Tectonophysics*, *367*, 235–251.

Fernandes, R. M. S., B. A. C. Ambrosius, R. Noomen, L. Bastos, M. J. R. Wortel, W. Spakman, and R. Govers (2003), The relative motion between Africa and Eurasia as derived from ITRF2000 and GPS data, *Geophys. Res. Lett.*, *30*(16), 1828, doi:10.1029/2003GL017089.

Flesch, L. M., W. E. Holt, A. J. Haines, and T. B. Shen (2000), Dynamics of the Pacific-North American plate boundary in the western United States, *Science*, *287*, 834–836.

Flesch, L. M., A. J. Haines, and W. E. Holt (2001), Dynamics of the India-Eurasia collision zone, *J. Geophys. Res.*, *106*, 16,435–16,460.

Fry, N. (2001), Stress space: Striated faults, deformation twins, and their constraints on palaeostress, *J. Struct. Geol.*, *23*, 1–9.

Galindo-Zaldívar, J., F. González Lodeiro, and A. Jabaloy (1993), Stress and paleostress in the Betic-Rif Cordilleras (Miocene to present-day), *Tectonophysics*, *227*, 105–126.

Galindo-Zaldívar, J., A. Jabaloy, F. González-Lodeiro, and F. Aldaya (1997), Crustal structure of the central sector of the Betic Cordillera (SE Spain), *Tectonics*, *16*, 18–37.

Galindo-Zaldívar, J., A. Jabaloy, I. Serrano, J. Morales, F. González Lodeiro, and F. Torcal (1999), Recent and present-day stresses in the Granada Basin (Betic Cordilleras): Example of a late Miocene-present-day extensional basin in a convergent plate boundary, *Tectonics*, *18*, 686–702.

Galindo-Zaldívar, J., A. J. Gil, M. J. Borque, F. González Lodeiro, A. Jabaloy, C. Marín Lechado, P. Ruano, and C. Sanz de Galdeano (2003), Active faulting in the internal zones of the central Betic Cordilleras (SE, Spain), *J. Geodyn.*, *36*, 239–250.

Gallart, J., J. Díaz, N. Vidal, and J. J. Dañobeitia (1995), The base of the crust at the Betics-Alborán Sea transition: Evidence for and abrupt structural variation from wide-angle ESCI Data, *Rev. Soc. Geol. Esp.*, *8*, 519–527.

García-Castellanos, D., M. Fernàndez, and M. Torne (2002), Modeling the evolution of the Guadalquivir foreland basin (southern Spain), *Tectonics*, *21*(3), 1018, doi:10.1029/2001TC001339.

García-Dueñas, V., J. C. Balanyá, and J. M. Martínez-Martínez (1992), Miocene extensional detachments in the outcropping basement of the northern Alboran basin (Betics) and their tectonic implications, *Geo Mar. Lett.*, *12*, 88–95.

García-Dueñas, V., E. Banda, M. Torné, D. Córdoba, and ESCI-Béticas Working Group (1994), A deep seismic reflection survey across the Betic Chain (southern Spain): First results, *Tectonophysics*, *232*, 77–89.

Gràcia, E., R. Pallàs, J. I. Soto, M. C. Comas, X. Moreno, E. Masana, P. Santanach, S. Diez, M. García, J. J. Dañobeitia, and HITS Scientific Party (2006), Active faulting offshore SE Spain (Alboran Sea): Implications for earthquake hazard assessment in the southern Iberian Margin, *Earth Planet. Sci. Lett.*, *241*, 734–749.

Grimison, N. L., and W. P. Chen (1986), The Azores-Gibraltar plate boundary: Focal mechanisms, depth of earthquakes, and their tectonic implications, *J. Geophys. Res.*, *91*, 2029–2047.

Gueguen, E., C. Doglioni, and M. Fernàndez (1998), On the post-25 Ma geodynamic evolution of the western Mediterranean, *Tectonophysics*, *298*, 259–269.

Gurría, E., and J. Mezcua (2000), Seismic tomography of the crust and lithospheric mantle in the Betic Cordillera and Alboran Sea, *Tectonophysics*, *329*, 99–119.

Gutscher, M. A., N. Kukowski, J. Malavielle, and S. Lallemand (1996), Cyclical behaviour of thrust wedges: Insights from high basal friction sandbox experiments, *Geology*, *24*, 135–138.

Gutscher, M. A., J. Malod, J. P. Rehault, I. Contrucci, F. Klingelhoefer, L. Mendes-Victor, and W. Spakman (2002), Evidence for active subduction beneath Gibraltar, *Geology*, *30*, 1071–1074.

Hahou, Y., N. Jabour, D. Oukemeni, M. El-Wartiti, and C. Nakhcha (2004), The earthquake of 26 May 1994, Al Hoceima, Morocco: Intensity distribution and macroseismic epicenter, *Seismol. Res. Lett.*, *75*, 46–53.

Haimson, B. C., and C. Fairhurst (1967), Initiation and extension of hydraulic fractures in rock, *Soc. Petrol. Eng. J.*, *7*, 310–318.

Heidbach, O., and J. Höhne (2004), CASMI—An interactive software tool for stress map plotting using the World Stress Map database. (Available online at http://www.world-stress-map.org)

Henares, J., C. López Casado, C. Sanz de Galdeano, J. Delgado, and J. A. Peláez (2003), Stress field in the Iberian-Magherbi region, *J. Seismol.*, *7*, 65–78.

Houseman, G. A., and P. C. England (1993), Crustal thickening versus lateral expulsion in the Indian-Asian continental collision, *J. Geophys. Res.*, *98*, 12,233–12,249.

Jackson, J. (1994), Active tectonics of the Aegean region, *Annu. Rev. Earth Planet. Sci.*, *22*, 239–271.

Jackson, J., and D. P. McKenzie (1988), Rates of active deformation in the Aegean Sea and surrounding areas, *Basin Res.*, *1*, 121–128.

Jiménez-Munt, I., and A. Negredo (2003), Neotectonic modeling of the western part of the Africa-Eurasia plate boundary: From the Mid-Atlantic Ridge to Algeria, *Earth Planet. Sci. Lett.*, *205*, 257–271.

Jiménez-Munt, I., P. Bird, and M. Fernández (2001), Thin-shell modeling of neotectonics in the Azores-Gibraltar region, *Geophys. Res. Lett.*, *28*, 1083–1086.

Jiménez-Munt, I., D. García-Castellanos, and M. Fernàndez (2005), Thin-sheet modeling of lithospheric deformation and surface mass transport, *Tectonophysics*, *407*, 239–255.

Jolivet, L., and C. Faccenna (2000), Mediterranean extension and the Africa-Eurasia collision, *Tectonics*, *19*, 1095–1106.

Jurado, M. J., and M. C. Comas (1992), Well log interpretation and seismic character of the Cenozoic sequence in the northern Alboran Sea, *Geo Mar. Lett.*, *12*, 129–136.

Kastrup, U., M. L. Zoback, N. Diechmann, K. F. Evans, D. Giardini, and J. M. Andrew (2004), Stress field variations in the Swiss Alps and the northern Alpine foreland derived from inversion of fault plane solutions, *J. Geophys. Res.*, *109*, B01402, doi:10.1029/2003JB002550.

Keller, J. V. A., S. H. Hall, C. J. Dart, and K. R. McClay (1995), The geometry and evolution of a transpressional strike-slip system: The Carboneras fault, SE Spain, *J. Geol. Soc. London*, *152*, 339–351.

Khazaradze, G., and J. Klotz (2003), Short- and long-term effects of GPS measured crustal deformation rates along the south central Andes, *J. Geophys. Res.*, *108*(B6), 2289, doi:10.1029/2002JB001879.

Kovác, M., M. Bielik, J. Hók, P. Kovác, B. Kronome, P. Labák, P. Moczo, D. Plasienka, J. Sefara, and M. Sujan (2002), Seismic activity and neotectonic evolution of the western Carpathians (Slovakia), in *Neotectonics and Surface Processes: The Pannonian Basin and Alpine/Carpathian System*, *Stephan Mueller Spec. Publ. Ser.*, vol. 3, edited by S. Cloetingh et al., pp. 295, Eur. Geophys. Union, Strasbourg, France.

Kreemer, C., and W. E. Holt (2001), A no-net-rotation model of present day surface motion, *Geophys. Res. Lett.*, *28*, 4407–4410.

Leblanc, D., and P. Olivier (1984), Role of strike-slip faults in the Betic-Rifian orogeny, *Tectonophysics*, *101*, 345–355.

Lonergan, L., and N. White (1997), Origin of the Betic-Rif mountain belt, *Tectonics*, *16*, 504–522.

López Casado, C., C. Sanz de Galdeano, S. Molina Palacios, and J. Henares Romero (2001), The structure of the Alboran Sea: Interpretation from seismological and geological data, *Tectonophysics*, *338*, 79–95.

Mardia, K. V. (1972), *Statistics of Directional Data*, pp. 357, Academic, San Diego, Calif.

Marín-Lechado, C., J. Galindo-Zaldívar, L. R. Rodríguez-Fernández, I. Serrano, and A. Pedrera (2005), Active faults, seismicity and stresses in an internal boundary of a tectonic arc (Campo de Dalías and Níjar, southeastern Betic Cordilleras, Spain), *Tectonophysics*, *396*, 81–96.

Marrett, R., and R. W. Allmendinger (1990), Kinematic analysis of fault-slip data, *J. Struct. Geol.*, *12*, 973–986.

Martínez-Díaz, J. J. (2002), Stress field variation related to fault reactivation in a reverse oblique-slip fault: The Alhama de Murcia fault, Betic Cordillera, Spain, *Tectonophysics*, *356*, 291–305.

Martínez-Díaz, J. J., and P. Hernández-Enrile (2004), Neotectonics and morphotectonics of the southern Almería region (Betic Cordillera-Spain) kinematic implications, *Int. J. Earth Sci.*, *93*, 189–206.

Martínez-Martínez, J. M., and J. M. Azañon (1997), Mode of extensional tectonics in the southeastern Betics (SE Spain): Implications for the

tectonic evolution of the peri-Alborán orogenic system, *Tectonics*, *16*, 205–225.

Martínez-Martínez, J. M., J. I. Soto, and J. C. Balanyá (2002), Orthogonal folding of extensional detachments: Structure and origin of the Sierra Nevada elongated dome (Betics, SE Spain), *Tectonics*, *21*(3), 1012, doi:10.1029/2001TC001283.

Masana, E., J. J. Martínez-Díaz, P. Hernández-Enrile, and P. Santanach (2004), The Alhama de Murcia fault (SE Spain), a seismogenic fault in a diffuse plate boundary: Seismotectonic implications for the Ibero-Magrebian region, *J. Geophys. Res.*, *109*, B01301, doi:10.1029/2002JB002359.

Mattei, M., F. Cifelli, I. M. Rojas, A. Crespo Blanc, M. Comas, and C. Faccenna y M. Porreca (2006), Neogene tectonic evolution of the Gibraltar Arc: New paleomagnetic constrains from the Betic chain, *Earth Planet. Sci. Lett.*, *250*, 522–540.

Mauffret, A., D. Frizon de Lamotte, S. Lallemant, C. Gorini, and A. Maillard (2004), E–W opening of the Algerian Basin (western Mediterranean), *Terra Nova*, *16*, 257–264.

McClusky, S., R. Reilinger, S. Mahmoud, D. Ben Sari, and A. Tealeb (2003), GPS constraints on Africa (Nubia) and Arabia plate motions, *Geophys. J. Int.*, *155*, 126–138.

McKenzie, D. P. (1972), Active tectonics of the Mediterranean region, *Geophys. J. R. Astron. Soc.*, *30*, 109–185.

Medina, F. (1995), Present-day state of stress in northern Morocco from focal mechanism analysis, *J. Struct. Geol.*, *17*, 1035–1046.

Meghraoui, M., S. Maouche, B. Chemaa, Z. Cakir, A. Aoudia, A. Harbi, P. J. Alasset, A. Ayadi, Y. Bouhadad, and F. Benhamouda (2004), Coastal uplift and thrust faulting associated with the $M_w = 6.8$ Zemmouri (Algeria) earthquake of 21 May 2003, *Geophys. Res. Lett.*, *31*, L19605, doi:10.1029/2004GL020466.

Meijer, P. T., R. Govers, and M. J. R. Wortel (1997), Forces controlling the present-day state of stress in the Andes, *Earth Planet. Sci. Lett.*, *148*, 157–170.

Mercier, J. L., D. Sorel, P. Vergely, and K. Simeakis (1989), Extensional tectonic regimes in the Aegean basins during the Cenozoic, *Basin Res.*, *2*, 49–71.

Mezcua, J., and J. Rueda (1997), Seismological evidence for a delamination process in the lithosphere under the Alboran Sea, *Geophys. J. Int.*, *129*, F1–F8.

Miller, S. A. (2002), Earthquake scaling and the strength of seismogenic faults, *Geophys. Res. Lett.*, *29*(10), 1389, doi:10.1029/2001GL014181.

Mitra, S. (1987), Regional variations in deformation mechanisms and structural styles in the central Appalachian orogenic belt, *Geol. Soc. Am. Bull.*, *98*, 569–590.

Molnar, P., and H. Lyon-Caen (1988), Some simple physical aspects of the support, structure, and evolution of mountain belts, in *Processes in Continental Lithospheric Deformation*, edited by S. P. Clark Jr., B. C. Burchfiel, and J. Suppe, *Spec. Pap. Geol. Soc. Am.*, *218*, 179–207.

Montenat, C. (1990), Les Bassins Néogènes du Domaine Betique Oriental (Espagne). Tectonique et sedimentation dans un couloir de decrochement, *Doc. Trav. IGAL*, *12–13*, 392 pp.

Montenat, C., and P. Ott d'Estevou (1995), Late Neogene basins evolving in the Eastern Betic transcurrent fault zone: An illustrated review, in *Tertiary Basins of Spain, the Stratigraphic Record of Crustal Kinematics*, edited by P. F. Friend and C. J. Dabrío, pp. 372–386, Cambridge Univ. Press, London.

Montenat, C. H., P. Ott d'Estevou, and P. Masse (1987), Tectonic-sedimentary characters of the Betic Neogene basins evolving in a crustal transcurrent shear zone (SE Spain), *Bull. Cent. Rech. Explor. Prod. Elf Aquitaine*, *11*, 1–22.

Montone, P., M. T. Mariucci, S. Pondrelli, and A. Amato (2004), An improved stress map for Italy and surrounding regions (central Mediterranean), *J. Geophys. Res.*, *109*, B10410, doi:10.1029/2003JB002703.

Morales, J., I. Serrano, A. Jabaloy, J. Galindo-Zaldívar, D. Zhao, F. Torcal, F. Vidal, and F. González-Lodeiro (1999), Active continental subduction beneath the Betic Cordillera and the Alborán Sea, *Geology*, *27*, 735–738.

Morel, J. L., and M. Meghraoui (1996), Goringe-Alboran-Tell tectonic zone: A transpression system along the Africa-Eurasia plate boundary, *Geology*, *24*, 755–758.

Negredo, A. M., P. Bird, C. Sanz de Galdeano, and E. Buforn (2002), Neotectonic modeling of the Ibero-Maghrebian region, *J. Geophys. Res.*, *107*(B11), 2292, doi:10.1029/2001JB000743.

Nocquet, J. M., and E. Calais (2003), Crustal velocity field of western Europe from permanent GPS array solutions, *Geophys. J. Int.*, *154*, 72–88.

Nocquet, J. M., and E. Calais (2004), Geodetic measurements of crustal deformation in the western Mediterranean and Europe, *Pure Appl. Geophys.*, *161*, 661–681.

Nocquet, J. M., E. Calais, Z. Altamimi, P. Sillard, and C. Boucher (2001), Intraplate deformation in western Europe deduced from an analysis of the ITRF97 velocity field, *J. Geophys. Res.*, *106*, 11,239–11,258.

Ott d'Estevou, P., and C. Montenat (1985), Evolution structurale de la zone Betique orientale (Espagne) du Tortonian à l'Holocène, *C. R. Acad. Sci.*, *300*, 363–368.

Piromallo, C., and A. Morelli (2003), *P* wave tomography of the mantle under the Alpine-Mediterranean area, *J. Geophys. Res.*, *108*(B2), 2065, doi:10.1029/2002JB001757.

Platt, J. P., and R. L. M. Vissers (1989), Extensional collapse of thickened continental lithosphere: A working hypothesis for the Alboran Sea and Gibraltar arc, *Geology*, *29*, 299–302.

Platt, J. P., J. I. Soto, M. J. Whitehouse, A. J. Hurford, and S. P. Kelley (1998), Thermal evolution, rate of exhumation, and tectonic significance of metamorphic rocks from the floor of the Alboran extensional basin, western Mediterranean, *Tectonics*, *17*, 671–689.

Platt, J. P., S. Allerton, A. Kirker, C. Mandeville, A. Mayfield, E. S. Platzman, and A. Rimi (2003), The ultimate arc: Differential displacement, oroclinal bending, and vertical axis rotation in the External Betic-Rif arc, *Tectonics*, *22*(3), 1017, doi:10.1029/2001TC001321.

Plumb, R. A., and S. H. Hickman (1985), Stress-induced borehole elongation: A comparison between the four-arm dipmeter and the borehole televiewer in the Auburn geothermal well, *J. Geophys. Res.*, *90*, 5513–5521.

Pollard, D. D., and P. Segall (1987), Theoretical displacements and stresses near fractures in rock: With applications to faults, joints, veins, dikes, and solution surfaces, in *Fracture Mechanics of Rock*, edited by B. K. Atkinson, pp. 277–349, Pergamon, London.

Polyak, B. G., et al. (1996), Heat flow in the Alboran Sea, western Mediterranean, *Tectonophysics*, *263*, 191–218.

Rebai, S., H. Philip, and A. Taboada (1992), Modern tectonic stress field in the Mediterranean region: Evidence for variation in stress directions at different scales, *Geophys. J. Int.*, *110*, 106–140.

Reicherter, K., and S. Reiss (2001), The Carboneras Fault Zone (southeastern Spain) revisited with ground penetrating radar—Quaternary structural styles from high-resolution images, *Neth. J. Geol.*, *80*, 129–138.

Reicherter, K. R., A. Jabaloy, J. Galindo-Zaldívar, P. Ruano, P. Becker-Heidmann, J. Morales, R. Reiss, and F. González-Lodeiro (2003), Repeated palaeoseismic activity of the Ventas de Zafarraya fault (S Spain) and its relation with the 1884 Andalusian earthquake, *Int. J. Earth Sci.*, *92*, 912–922.

Reilly, W. I., G. Fredrich, G. W. Mein, H. Landau, J. L. Almazan, and J. L. Caturla (1992), Geodetic determination of crustal deformation across the Strait of Gibraltar, *Geophys. J. Int.*, *111*, 391–398.

Rosenbaum, G., G. S. Lister, and C. Duboz (2002), Relative motions of Africa, Iberia and Europe during Alpine orogeny, *Tectonophysics*, *359*, 117–129.

Roy, M., and L. H. Royden (2000), Crustal rheology and faulting at strike-slip plate boundaries: 1. An analytic model, *J. Geophys. Res.*, *105*, 5583–5597.

Royden, L. H. (1993), The tectonic expression of slab pull at continental convergent boundaries, *Tectonics*, *12*, 303–325.

Saji, R., and A. Chalouan (1995), Le Bassin pliocène intramontagneux de Tirinesse et son mode d'ouverture (Rif interne, Maroc), *Geogaceta*, *17*, 110–112.

Sánchez-Gómez, M., and F. Torcal (2002), Recent tectonic activity on the south margin of the Guadalquivir basin, between Cabra and Quesada towns (provinces of Jaén and Córdoba, Spain), in *I Centenario del Observatorio de Cartuja*, Abstract book, pp. 59–60, Inst. Andaluz de Geofis., Univ. de Granada, Granada, Spain.

Sanz de Galdeano, C. (1990), Geologic evolution of the Betic Cordilleras in the western Mediterranean, Miocene to the Present, *Tectonophysics*, *172*, 107–119.

Sanz de Galdeano, C., C. López Casado, J. Delgado, and M. A. Peinado (1995), Shallow seismicity and active faults in the Betic Cordillera. A preliminary approach to seismic sources associated with specific faults, *Tectonophysics*, *248*, 293–302.

Scholz, C. (2000), Evidence for a strong San Andreas fault, *Geology*, *28*, 163–166.

Seber, D., M. Barazangi, A. Ibenbrahim, and A. Demnati (1996a), Geophysical evidence for lithospheric delamination beneath the Alboran Sea and Rif-Betic Mountains, *Nature*, *379*, 785–790.

Seber, D., M. Barazangi, B. A. Tadili, F. Ramdani, A. Ibenbrahim, and D. B. Sari (1996b), Three-dimensional upper mantle structure beneath the intraplate Atlas and interplate Rif Mountains of Morocco, *J. Geophys. Res.*, *101*, 3125–3138.

Sella, G. F., T. H. Dixon, and A. Mao (2002), REVEL: A model for Recent plate velocities from space geodesy, *J. Geophys. Res.*, *107*(B4), 2081, doi:10.1029/2000JB000033.

Selverstone, J. (2005), Are the Alps collapsing?, *Annu. Rev. Earth Planet. Sci.*, *33*, 113–132.

Serrano, I., T. M. Hearn, J. Morales, and F. Torcal (2005), Seismic anisotropy and velocity structure beneath the southern half of the Iberian Peninsula, *Phys. Earth Planet. Inter.*, *150*, 317–330.

Shamir, G., and M. D. Zoback (1992), Stress orientation profile to 3.5 km depth near the San Andreas fault at Cajon Pass, California, *J. Geophys. Res.*, *97*, 5059–5080.

Sonder, L. J. (1990), Effects of density contrasts on the orientation of stresses in the lithosphere: Relation to principal stress directions in the Transverse ranges, California, *Tectonics*, *9*, 761–771.

Soto, J. I., and F. J. Manzano (2002), Geometría y cinemática de fallas recientes en el margen septentrional del Mar de Alborán (Sector de Maro, Provincia de Málaga), *Geogaceta*, *31*, 139–142.

Soto, J. I., M. C. Comas, and J. de la Linde (1996), Espesor de sedimentos en la cuenca de Alborán mediante una conversión sísmica corregida, *Geogaceta*, *20*, 382–385.

Spakman, W., and M. J. R. Wortel (2004), A tomographic view on western Mediterranean geodynamics, in *The TRANSMED Atlas: The Mediterranean Region From Crust to Mantle*, edited by W. Cavazza et al., pp. 31–52, Springer, Berlin, Germany.

Stein, C. A., S. Cloetingh, and R. Wortel (1989), Seasat-derived gravity constraints on stress and deformation in the northeastern Indian Ocean, *Geophys. Res. Lett.*, *16*, 823–826.

Stich, D., C. J. Ammon, and J. Morales (2003), Moment tensor solutions for small and moderate earthquakes in the Ibero-Maghreb region, *J. Geophys. Res.*, *108*(B3), 2148, doi:10.1029/2002JB002057.

Stich, D., F. de L. Mancilla, D. Baumont, and J. Morales (2005), Source analysis of the M_w 6.3 2004 Al Hoceima earthquake (Morocco) using regional apparent source time functions, *J. Geophys. Res.*, *110*, B06306, doi:10.1029/2004JB003366.

Stich, D., E. Serpelloni, F. L. Mancilla, and J. Morales (2006), Kinematics of the Iberia-Maghreb plate contact from seismic moment tensors and GPS observations, *Tectonophysics*, *426*, 295–317.

Torne, M., and E. Banda (1992), Crustal thinning from the Betic Cordillera to the Alboran Sea, *Geo Mar. Lett.*, *12*, 76–81.

Torne, M., E. Banda, V. García-Dueñas, and J. C. Balanyá (1992), Mantle-lithosphere bodies in the Alboran crustal domain (Ronda peridotites, Betic-Rif orogenic belt), *Earth Planet. Sci. Lett.*, *110*, 163–171.

Torne, M., M. Fernàndez, M. C. Comas, and J. I. Soto (2000), Lithospheric structure beneath the Alboran Basin: Results from three-dimensional gravity modeling and tectonic relevance, *J. Geophys. Res.*, *105*, 3209–3228.

Townend, J., and M. D. Zoback (2000), How faulting keeps the crust strong, *Geology*, *28*, 399–402.

Turner, F. J. (1953), Nature and dynamic interpretation of deformation lamellae in calcite of 3 marbles, *Am. J. Sci.*, *251*, 276–298.

Twiss, R. J., and J. R. Unruh (1998), Analysis of fault slip inversions: Do they constrain stress or strain rate?, *J. Geophys. Res.*, *103*, 12,205–12,222.

Udías, A., and E. Buforn (1991), Regional stresses along the Eurasia-Africa plate boundary derived from focal mechanisms of large earthquakes, *Pure Appl. Geophys.*, *136*, 433–448.

Udías, A., and D. Muñoz (1979), The Andalusian earthquake of 25 December 1884, *Tectonophysics*, *53*, 291–299.

Walcott, R. I. (1972), Gravity, flexure and the growth of sedimentary basins at a continental edge, *Geol. Soc. Am. Bull*, *83*, 1845–1848.

Watts, A. B., J. P. Platt, and M. L. Buhl (1993), Tectonic evolution of the Alboran Sea Basin, *Basin Res.*, *5*, 153–177.

Weijermars, R. (1987), The Palomares brittle-ductile shear zone of southern Spain, *J. Struct. Geol.*, *9*, 139–158.

Working Group for Deep Seismic Sounding in the Alboran Sea 1974 (1978), Crustal seismic profiles in the Alboran Sea: Preliminary results, *Pure Appl. Geophys.*, *116*, 167–180.

Wortel, M. J. R., and W. Spakman (2000), Subduction and slab detachment in the Mediterranean-Carpathian region, *Science*, *290*, 1910–1917.

Yelles, K., K. Lammali, A. Mahsas, E. Calais, and P. Briole (2004), Coseismic deformation of the May 21st, 2003, M_w = 6.8 Boumerdes earthquake, Algeria, from GPS measurements, *Geophys. Res. Lett.*, *31*, L13610, doi:10.1029/2004GL019884.

Ziegler, P. A., and P. Dèzes (2006), Crustal evolution of western and central Europe, in *European Lithosphere Dynamics*, edited by D. G. Gee and R. A. Stephenson, *Mem. Geol. Society London*, *32*, 43–56.

Zizi, M. (2002), Triassic-Jurassic extensional systems and their Neogene reactivation in Northern Morocco: The rides Prerifaines and Guercif basin, *Notes Mem. Serv. Geol. Maroc*, *416*, 138.

Zoback, M. D., and M. L. Zoback (1989), Regional tectonic stress field of the continental U.S., in *Geophysical Framework of the Continental United States*, edited by L. Pakiser and W. D. Mooney, *Mem. Geol. Soc. Am.*, *172*, 523–539.

Zoback, M. D., and M. L. Zoback (1991), Tectonic stress field of North America and relative plate motions, in *Neotectonics of North America*, Decade Map vol. 1, edited by D. B. Slemmons et al., pp. 339–366, Geol. Soc. of Am., Boulder, Colo.

Zoback, M. D., D. Moos, L. Mastin, and R. N. Anderson (1985), Wellbore breakouts and in situ stress, *J. Geophys. Res.*, *90*, 5523–5530.

Zoback, M. D., et al. (1987), New evidence on the state of stress of the San Andreas fault system, *Science*, *238*, 1105–1111.

Zoback, M. D., C. A. Barton, M. Brudy, D. A. Castillo, T. Finkbeiner, B. R. Grollimund, D. B. Moos, P. Peska, C. D. Ward, and D. J. Wiprut (2003), Determination of stress orientation and magnitude in deep wells, *Int. J. Rock Mech. Min.*, *40*, 1049–1076.

Zoback, M. L. (1992), First- and second-order patterns of stress in the lithosphere: The World Stress Map Project, *J. Geophys. Res.*, *90*, 11,703–11,728.

Zoback, M. L., and W. D. Mooney (2003), Lithospheric buoyancy and continental intraplate stresses, *Int. Geol. Rev.*, *45*, 95–118.

Zoback, M. L., et al. (1989), Global patterns of intraplate stresses: A status report on the World Stress Map Project of the International Lithosphere Program, *Nature*, *341*, 291–298.

Zouhri, L., C. Lamouroux, D. Vachard, and A. Pique (2002), Evidence of flexural extension of the Rif foreland: The Rharb-Mamora basin (northern Morocco), *Bull. Soc. Geol. Fr.*, *173*, 509–513.

F. Fernández-Ibáñez and J. I. Soto, Instituto Andaluz de Ciencias de la Tierra, Universidad de Granada, Campus Fuentenueva s/n, E-18002 Granada, Spain. (fferiba@ugr.es; jsoto@ugr.es)

J. Morales, Instituto Andaluz de Geofísica, Universidad de Granada, E-18071 Granada, Spain. (morales@iag.ugr.es)

M. D. Zoback, Department of Geophysics, Stanford University, Stanford, CA 94305-2215, USA. (zoback@pangea.stanford.edu)